ARMY RESEARCH LABORATORY

Modifications to the XBR-2D Heat Conduction Code

Andrew B. Crickenberger
Robert L. Talley
James Q. Talley

ARL-CR-126 April 1994

prepared by

Veritay Technology, Inc.
4845 Millersport Highway
P.O. Box 305
East Amherst, NY 14051-0305

under contract

DAAA15-92-D-003

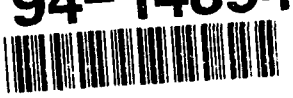

NOTICES

Destroy this report when it is no longer needed. DO NOT return it to the originator.

Additional copies of this report may be obtained from the National Technical Information Service, U.S. Department of Commerce, 5285 Port Royal Road, Springfield, VA 22161.

The findings of this report are not to be construed as an official Department of the Army position, unless so designated by other authorized documents.

The use of trade names or manufacturers' names in this report does not constitute indorsement of any commercial product.

REPORT DOCUMENTATION PAGE

Form Approved
OMB No. 0704-0188

1. AGENCY USE ONLY (Leave blank)	2. REPORT DATE	3. REPORT TYPE AND DATES COVERED
	April 1994	Final, Jun 92–Jun 93

4. TITLE AND SUBTITLE
Modifications to the XBR-2D Heat Conduction Code

5. FUNDING NUMBERS
C: DAAA15-92-D-003

6. AUTHOR(S)
Andrew B. Crickenberger, Robert L. Talley, and James Q. Talley

7. PERFORMING ORGANIZATION NAME(S) AND ADDRESS(ES)
Veritay Technology, Inc.
4845 Millersport Highway
P.O. Box 305
East Amherst, NY 14051-0305

8. PERFORMING ORGANIZATION REPORT NUMBER

9. SPONSORING/MONITORING AGENCY NAME(S) AND ADDRESS(ES)
U.S. Army Research Laboratory
ATTN: AMSRL-OP-AP-L
Aberdeen Proving Ground, MD 21005-5066

10. SPONSORING/MONITORING AGENCY REPORT NUMBER
ARL-CR-126

11. SUPPLEMENTARY NOTES

12a. DISTRIBUTION/AVAILABILITY STATEMENT
Approved for public release; distribution is unlimited.

12b. DISTRIBUTION CODE

13. ABSTRACT *(Maximum 200 words)*

A study was conducted to evaluate different methods to improve the execution speed of the XBR-2D heat conduction code. When run in burst fire mode, the original XBR-2D code could require up to 20 hours of CPU time on a Cray computer.

Two numerical methods were studied as alternatives to the explicit finite difference techniques employed in Version 1 of the code: an implicit finite difference method and a boundary element method (BEM). The BEM appeared to offer a promising and elegant approach to the solution of the heat conduction problem. A detailed explanation of the BEM is contained in this report; however, it was not implemented at this time because of its complexity.

The final solution inserted into the code was an improved explicit finite difference method. Under this mechanism the execution time was reduced by up to two-thirds. The speed increase was largely obtained through improvements in coding efficiency and the use of a variable time step based on the maximum temperature gradient in the system.

14. SUBJECT TERMS
numerical analysis, CRAY, implicit finite difference method, boundary element method, temperature gradients, explicit finite difference method, gun barrels

15. NUMBER OF PAGES
59

16. PRICE CODE

17. SECURITY CLASSIFICATION OF REPORT	18. SECURITY CLASSIFICATION OF THIS PAGE	19. SECURITY CLASSIFICATION OF ABSTRACT	20. LIMITATION OF ABSTRACT
UNCLASSIFIED	UNCLASSIFIED	UNCLASSIFIED	UL

INTENTIONALLY LEFT BLANK.

TABLE OF CONTENTS

INTENTIONALLY LEFT BLANK.

LIST OF FIGURES

INTENTIONALLY LEFT BLANK.

LIST OF TABLES

LIST OF TABLES

1. INTRODUCTION

The XBR-2D code is a two-dimensional (2-D), axisymmetric heat conduction code specially formulated and developed by Veritay Technology for the U.S. Army Ballistic Research Laboratory (now known as the Army Research Laboratory [ARL]) to simulate gun barrel heat transfer during single shot and burst firing scenarios*. The code is an explicit finite difference formulation that features a geometric radial grid network. This provides finely spaced grids at the bore surface to accurately model the steep temperature gradients at the time of maximum heat flux, while defining the temperature distribution through the barrel wall with a minimum number of grids.

The explicit nature of the formulation requires that the maximum value of the time interval be limited by specific criteria to maintain computational stability. Thus, the maximum time step is constrained by the thickness of the smallest grid.

The burst fire event consists of a number of brief ballistic cycle periods, which are generally less than 100 ms in duration and are characterized by intense heating and steep temperature gradients at the bore surface. These represent the most severe conditions that the code is designed to simulate. Between these periods of ballistic activity are dwell periods in which heat transfer is low and the through-wall thermal profile relaxes through heat conduction processes. The temperature gradient at the bore surface decreases in magnitude but the grid pattern remains extremely fine. Prior to this effort, the same time step and grid pattern were used throughout the simulation to evaluate both the brief ballistic cycle and the potentially extensive dwell period between shots. When simulating long burst fire scenarios for artillery with the original version of the XBR-2D code, the computer time is excessive; execution times of 20 hours on the ARL's Cray computer have been cited. Thus, it is desired to reduce the run time exhibited by the code while maintaining its computational accuracy.

1.1 Approaches to the Problem. Two possible approaches were evaluated to reduce the execution time. The first approach involved changing the numerical method to either an implicit finite difference or a boundary element method. An implicit finite difference scheme involves solving the entire grid matrix simultaneously for each time step as opposed to the explicit scheme which solves each grid independently based on the values at the previous time step. An advantage of the implicit method is that

*Developed under contract No. DAAA15-88-D-0014, Delivery Order 0004.

there are no stability-related time step restrictions. The main constraint on the time step is the need to maintain adequate resolution of the heat transfer time history. During the dwell period, the step can be increased without sacrificing accuracy. Using test cases designed to evaluate the different methods, the implicit finite difference solutions did not agree with the explicit method in any calculations. After reviewing both methods to verify that they were properly implemented, and calculating analytical solutions to the test cases, it was determined that the implicit method was not providing accurate solutions to the problems, so it was eliminated as an option.

The boundary element method (BEM) has the possibility of significantly improving the speed as well as the accuracy of the solution. The BEM solves the governing equation only along the boundary, eliminating the need to compute internal points. If internal values are desired, only the point of interest needs to be calculated. This eliminates the large number of extraneous internal points which need to be calculated in either of the finite difference methods. However, the BEM, especially for the case of transient heat conduction, involves very complicated mathematics in its derivation. Because of the limited scope of this task order, the BEM could not be pursued to its conclusion, although some very valuable and promising work was accomplished.

The second approach to speeding up the XBR-2D code, and the one that was ultimately implemented, was to work with the current explicit finite difference scheme and improve its efficiency. Since the time step in the original version of the code was constant for both the ballistic cycle and the dwell period, an increase in the step size for the dwell period (when the stability requirements are relaxed) allows for a decrease in the execution time. An algorithm was developed which computes the maximum temperature gradient in the system, and dynamically alters the time step based on this value. This algorithm, along with other programming optimizations, decreased the execution time by factors of three to six, depending upon the length of the dwell period. These improvements in the execution time were achieved without significantly affecting the numerical results of the XBR-2D simulations.

2. EVALUATION OF NUMERICAL ALTERNATIVES

To quickly evaluate the various numerical methods, two test cases were developed. Case one, illustrated in Figure 1, is a flat, two-dimensional, 6 × 6 plate with a constant temperature of 300° on one side and a constant temperature of 1,500° on the opposite side. The remaining sides are insulated. The steady-state solution to this problem is a linear distribution from 300 to 1,500.

The second test case is also illustrated in Figure 1. In this case, the plate from the first test case is insulated on three sides and a heat flux is applied to the fourth side. The heat flux is applied for 30 ms and is followed by a pause of 60 ms. The cycle is then repeated to roughly simulate the conditions in a gun barrel.

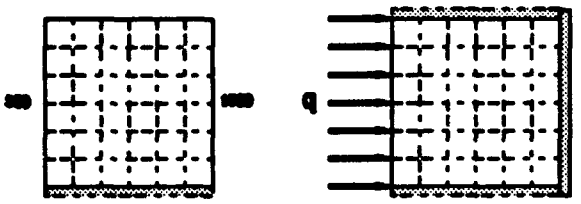

Figure 1. Heat transfer test cases used to evaluate various numerical techniques.

2.1 Explicit and Implicit Finite Difference Methods. The numerical method contained in XBR-2D version 1.0 is an explicit, centered finite difference method. This method is explained in detail in the original XBR-2D report (Chandra 1990). In an x-y coordinate system, the transient heat equation,

$$\Delta^2 T = \frac{1}{\alpha} \frac{\delta T}{\delta t} \quad , \tag{1}$$

can be modeled using this method with the centered difference equation

$$T_{i,j}^{n+1} = T_{i,j}^{n} + \alpha \Delta t \left(\frac{T_{i+1,j}^{n} - 2T_{i,j}^{n} + T_{i-1,j}^{n}}{\Delta x^2} + \frac{T_{i,j+1}^{n} - 2T_{i,j}^{n} + T_{i,j+1}^{n}}{\Delta y^2} \right) + \Delta t \dot{q} \quad , \tag{2}$$

$$\dot{q} = -k \frac{\Delta T}{\Delta x} = \text{Boundary Condition}$$

where $\dot{q}$ is the external heat flux at the grid, $T_{i,j}$ is the temperature of the grid of interest, and $T_{i,j+1}$, $T_{i,j-1}$, $T_{i+1,j}$, $T_{i-1,j}$ are the temperatures of adjacent grids.

The time step was varied with the explicit method until a converged solution was reached. This process is illustrated in Figures 2–4. Figure 2 shows the overall behavior of the first test case with various-sized time steps. Temperature differences with the larger time steps all occur in the very early region. Figures 3 and 4 focus on the early time behavior where the solutions converge as the step size is reduced. A time step of 0.010 s was chosen for the baseline calculations.

The results of the second test case are shown in Figure 5. For this case the explicit method was unstable if the time step was large, but, once the step was small enough to maintain stability, the results remained the same as the time step was reduced further. A step size of 0.001 s was chosen for the baseline calculations of Test Case No. 2.

These baseline solutions were then used to evaluate the accuracy of the implicit finite difference calculations.

The implicit finite difference method chosen to be evaluated was the alternating-direction implicit (ADI) method (Anderson, Tannehill, and Pletcher 1984). This method was chosen over standard centered difference implicit methods because it produces a tridiagonal system of equations. A tridiagonal matrix requires substantially less computational time to solve than nontridiagonal matrices such as those developed with standard implicit methods. The key to minimizing the execution time of the implicit method is the selection of an algorithm to solve the tridiagonal system of equations. Three tridiagonal matrix solving algorithms were evaluated: the Thomas algorithm (Anderson, Tannehill, and Pletcher 1984), Gauss-Jordan Elimination, and LU Decomposition (Press et al. 1989). The Thomas algorithm, found to be slightly faster than the other two, was chosen as the solution method. All three algorithms gave identical numerical results.

Figures 6 and 7 show a comparison between the explicit and implicit solutions for the two test cases. The figures show a distinct difference in the behavior of the implicit method. Both finite difference methods were re-examined and appeared to be implemented properly, but the solutions could not be made to agree. An analytical solution was developed for the second test case. When this solution was compared to the implicit and explicit results, it became obvious that the implicit method was not properly solving the problem. The implicit method was, therefore, eliminated as an option.

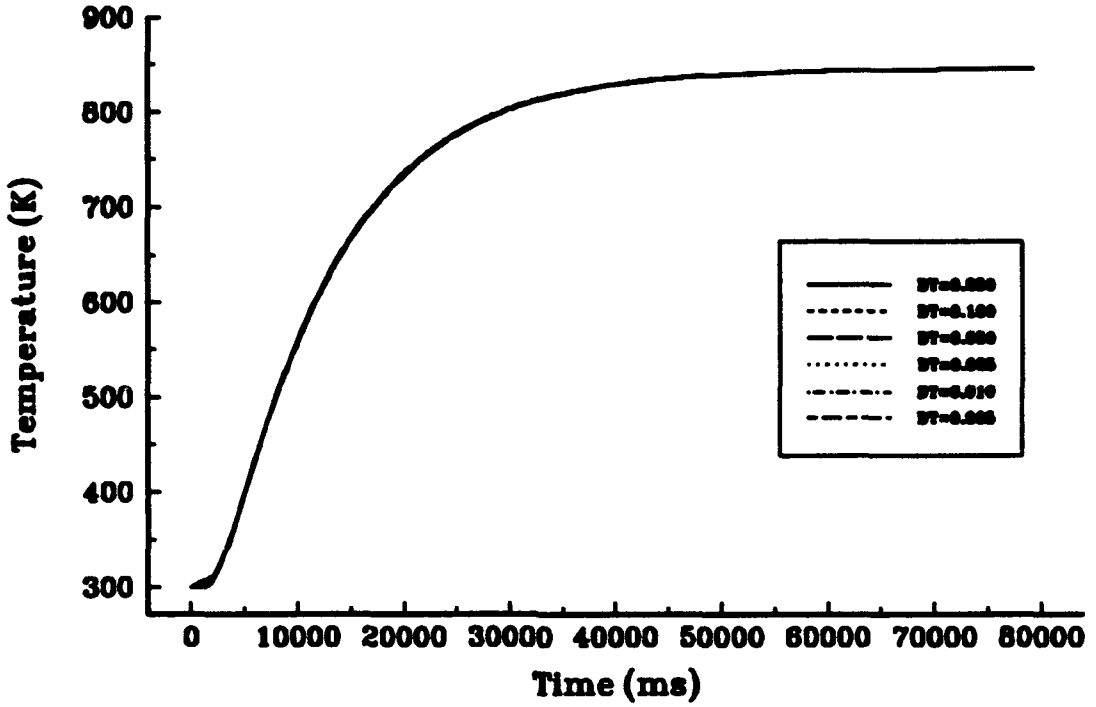

Figure 2. Comparison of various timesteps for the explicit Test Case No. 1. Temperature is taken at the center of the block.

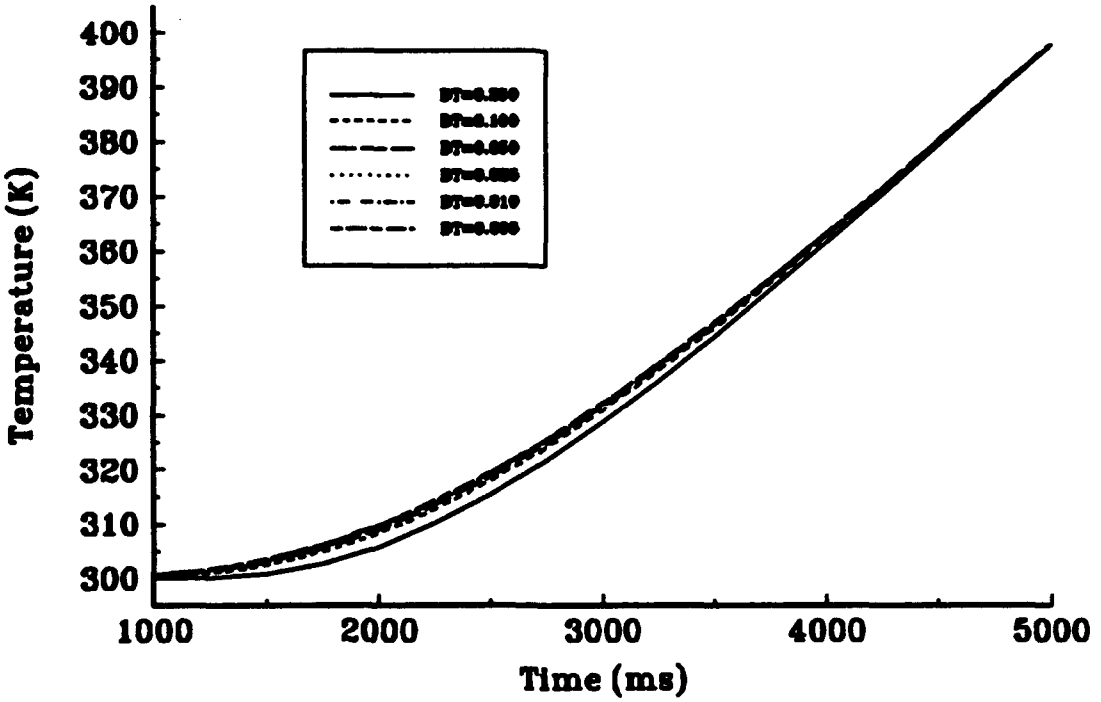

Figure 3. Early time behavior for the explicit Test Case No. 1.

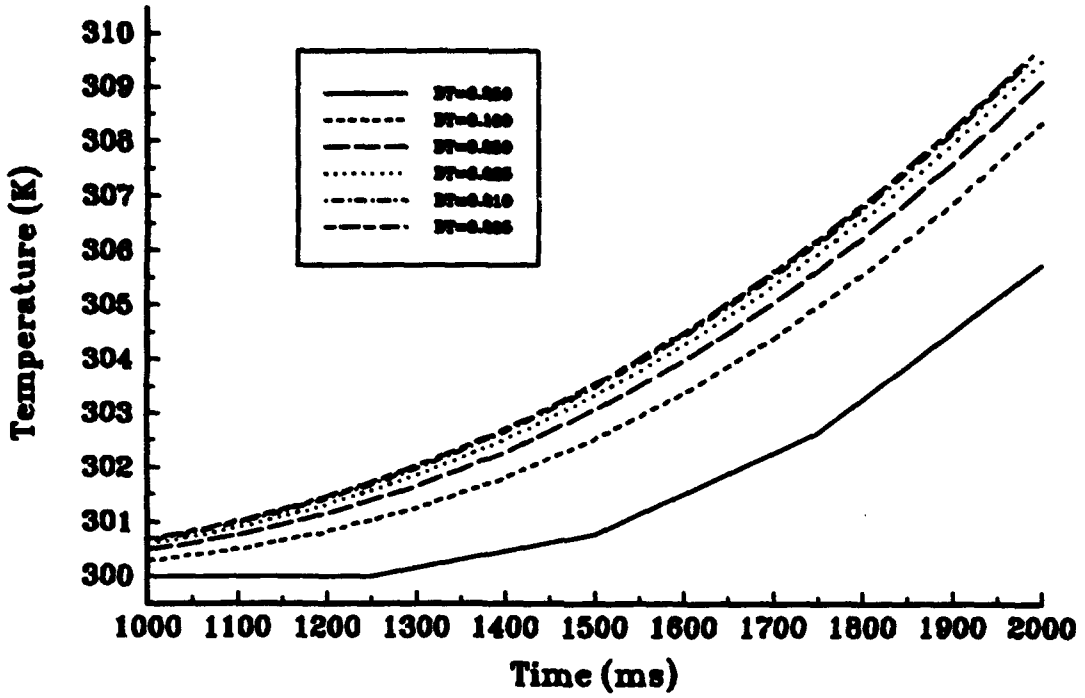

Figure 4. Early time behavior for various timesteps in the explicit Test Case No. 1.

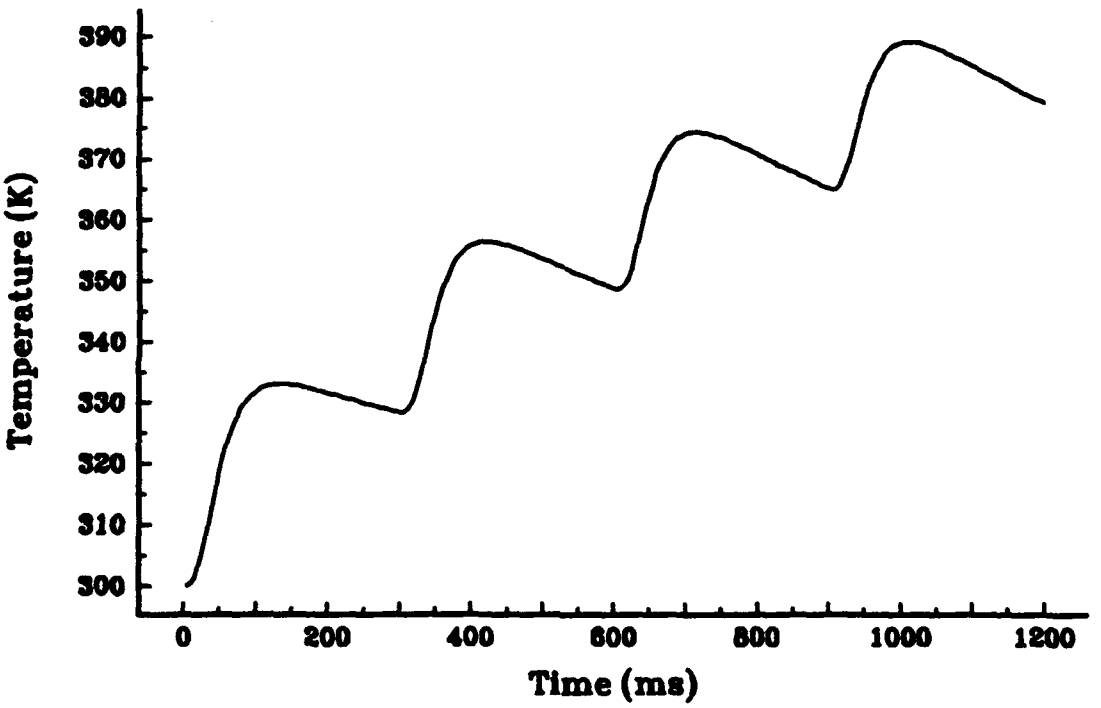

Figure 5. Temperatures at the center of the block for the explicit Test Case No. 2.

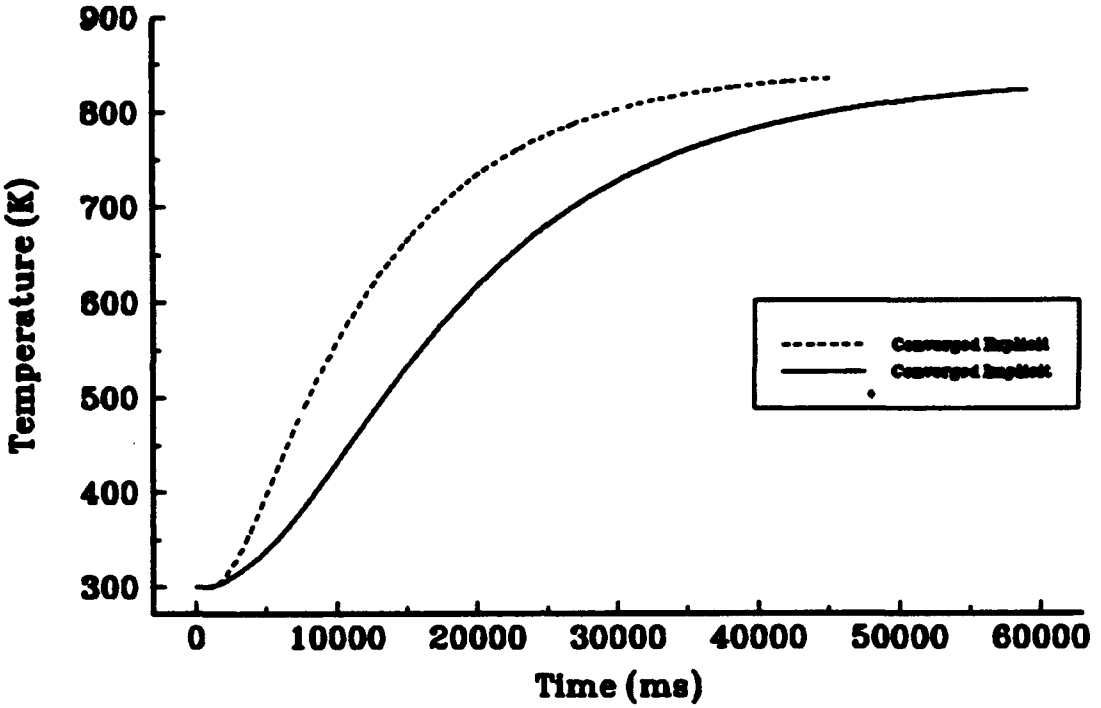

Figure 6. Comparison of the explicit and implicit solutions for Test Case No. 1.

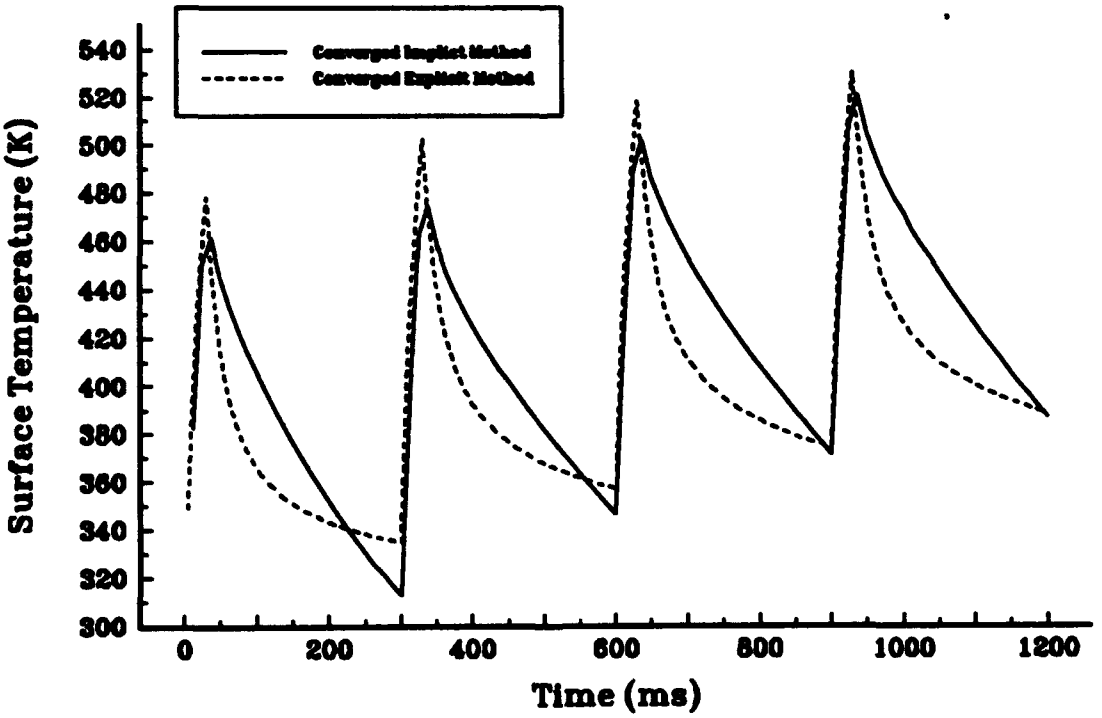

Figure 7. Comparison of the explicit and implicit solutions, at the surface, for Test Case No. 2.

2.2 Boundary Element Method (BEM). As the name implies, in the BEM approach the governing differential equations are transformed into integral identities which are applied on the boundary. These integrals are then numerically integrated over the boundary, which has been divided into small segments (boundary elements). The BEM can be applied to complex boundary shapes relatively easily and, furthermore, since all the approximations are restricted to the boundary, it can model regions having rapidly changing variables with considerable accuracy.

Since the problem is solved only on the boundary, and fewer calculations are involved, the BEM should provide a significant decrease in the execution time over either finite difference method. For the Poisson equation, (i.e., steady state heat conduction), the BEM formulation is well known and documented (Becker 1992; Brebbia and Dominguez 1989; Brebbia and Walker 1980). However, when a time dependency is added to the problem, the formulation becomes much more complex.

An existing steady state heat conduction BEM code, POLINBE (Brebbia and Dominguez 1989), was chosen for evaluation. This code was written to model problems with geometries similar to the test cases used to evaluate the finite difference techniques. When run as a steady state problem, a solution was obtained practically instantaneously.

Appendix A describes in detail the mathematical formulation of the transient heat conduction BEM. This formulation was added to the POLINBE code in an attempt to develop a transient BEM solution to model the test cases. Several problems where encountered in the formulation of the method. The most important difficulty was the selection of an approximation function. This function is a key element of the transient heat conduction formulation and further effort is required to determine an appropriate function for the barrel heating problem.

The BEM is quite complex, and development and implementation of this technique could not be accomplished during the present program; however, the progress that was made strongly suggests that it holds great potential. It is believed that this method may be able to provide a substantial decrease in execution time, while providing an increase in computational accuracy; however, these attributes have yet to be demonstrated for the barrel heat conduction problem.

3. XBR-2D CODE MODIFICATIONS

3.1 Time Step Changes. The test cases described in Section 2 illustrated the difficulties associated with achieving execution time improvements by altering the integration method. The sample cases were not able to maintain a consistent numerical solution without additional effort that would have required greater resources than were available. It was decided that the best option at this time was to improve the existing explicit finite difference method's efficiency by modifying the time step and optimizing the FORTRAN coding.

In the original version of the XBR-2D code, the time step (Δt) was based on the stability criteria:

$$\Delta t = \frac{\Delta r^2}{6\alpha} \tag{3}$$

For a barrel with a chrome plating, Δr was fixed at the plating thickness, otherwise Δr was determined based on a user-provided Δt. This time step is then used throughout the ballistic cycle and, in the case of multiple shots, the dwell period between shots. In cases where there is a significant dwell period, the temperature gradients can become quite small and a step as small as dictated by equation 3 is not necessary to maintain stability.

In a first attempt to speed up the code, the time step was increased equally for the entire dwell period. Any significant increase in the Δt caused the code to become unstable. To maintain stability, the time step modification was then changed to a function dependent upon the maximum radial temperature gradient in the system. In the dwell region, the step is defined as

$$\Delta t = \frac{\Delta t_{base}}{(\Delta T_r)_{max}} \; CF \tag{4}$$

where CF is a geometric correction factor which accounts for differences in grid sizes between various gun calibers, Δt_{base} is defined in equation 3, and $(\nabla T_r)_{max}$ is the maximum temperature gradient in the barrel. The dwell time step is restricted so that it cannot be smaller than the base time step, Δt_{base}, nor can it be greater than 100 times the base time step.

This correlation provides the largest increase in step size when the heat conduction approaches a steady state, and will provide the most substantial speed increases in multiple shot simulations where the length of the dwell period is long compared to the length of the ballistic cycle, as in the case of artillery.

3.2 Code Optimization. Many small code optimizations were also made in most of XBR-2D's subroutines. These involved replacing frequently used array elements (such as T(I+1)) with local variables (such as T1), replacing repetitive calculations with a single calculation, and moving certain calculations out of loops. These optimizations were most significant in the subroutine HEATRANS which carries out the finite difference calculations, and in the subroutines which calculate the boundary conditions. These modifications, on their own, decreased the execution time of XBR-2D by 15%.

An option that was included in the original XBR-2D was the ability to turn off the screen updates. By turning off the screen updates alone, the execution time on a PC decreases by 15%. For the comparisons done in the next section, the screen update was turned off for both the original XBR-2D runs and the new runs. All of the runs in the next section were calculated on a 33-MHz 80486 PC-compatible computer.

4. CODE EVALUATION

4.1 155-mm Howitzer. A 155-mm howitzer test case for Unicharge was provided by the ARL. This case simulates the firing of 60 rounds with a 5-s dwell time between each shot. Initially, to speed up the debugging and testing process, only the first round was studied. This case involved a single shot followed by a dwell of 5 s. Table 1 compares the bore surface temperature rise of this single shot case before and after the code modifications. Table 2 compares the peak bore surface temperature at each location. The values are unchanged for the two simulations. The modifications to the code do not take effect until after the peak temperature has been reached. The new code required less than 20% of the execution time required by version 1.0 of XBR-2D.

Figure 8 is a graph of the probe temperature for the new and old runs. The two cases are so close that any differences are not discernible on the graph.

Table 1. Comparison of Old and New XBR-2D Surface Temperature Rise for a Single-Shot 155-mm Test Case (Temperatures are at the Completion of the Simulation)

Run	Execution Time (s)	Temperature rise (K) at each location. Locations in inches from the breech end.							
		10.0	42.3	85.7	129.1	172.5	215.9	259.3	310.8
Orig	3,650	29.90	27.91	22.32	20.73	18.70	15.74	16.81	15.81
New	705	29.75	27.91	22.32	20.72	18.70	15.74	16.81	15.81

Table 2. Comparison of Old and New XBR-2D Peak Surface Temperature Rise for a Single-Shot 155-mm Test Case

Run	Execution Time (s)	Peak temperature rise (K) at each location. Locations in inches from the breech end.							
		10.0	42.3	85.7	129.1	172.5	215.9	259.3	310.8
Orig	3,650	883.3	1031.7	847.3	695.0	563.8	418.1	443.9	357.3
New	705	883.3	1031.7	847.3	695.0	563.8	418.1	443.9	357.3

Table 3 summarizes the results of the full 60-round simulation. Figures 9 and 10 are plots of the surface temperature rise and the probe temperature rise, respectively. There are no discernible differences on the graphs.

Table 3. Comparison of Old and New XBR-2D Surface Temperature Rise for a 60-Shot 155-mm Test Case (Temperatures are at the Completion of the Simulation)

Run	Execution Time (s)	Temperature rise (K) at each location. Locations in inches from the breech end.							
		10.0	42.3	85.7	129.1	172.5	215.9	259.3	310.8
Orig	264,819	373.5	368.0	312.2	275.4	242.3	202.4	213.7	202.0
New	78,144	372.5	367.7	311.3	274.7	241.8	202.0	213.3	201.6

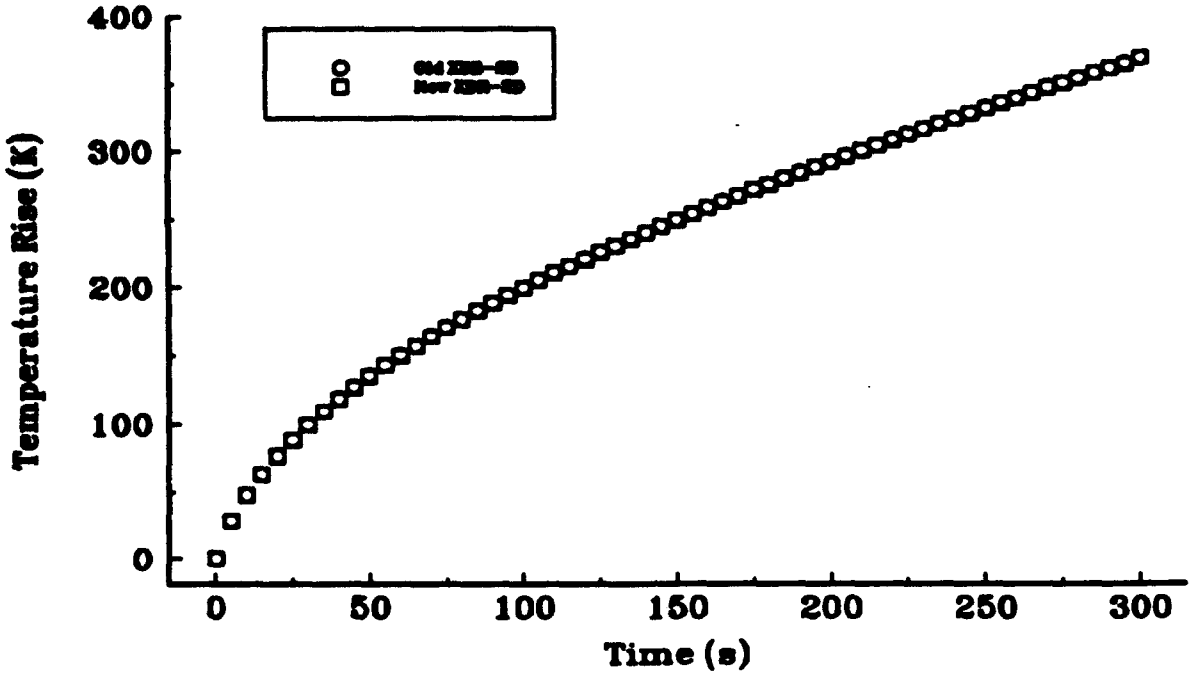

Figure 8. Residual bore surface temperature at 10 in after each shot in the 60-shot simulation.

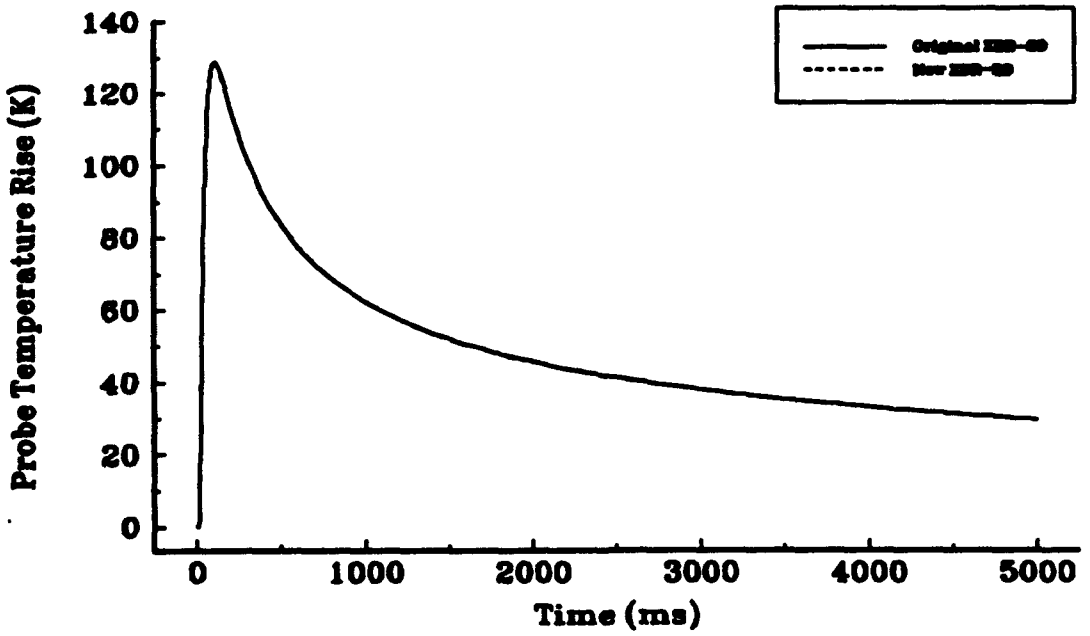

Figure 9. XBR-2D 155-mm howitzer comparison. Temperatures are at 10 in and a probe depth of 0.05 in.

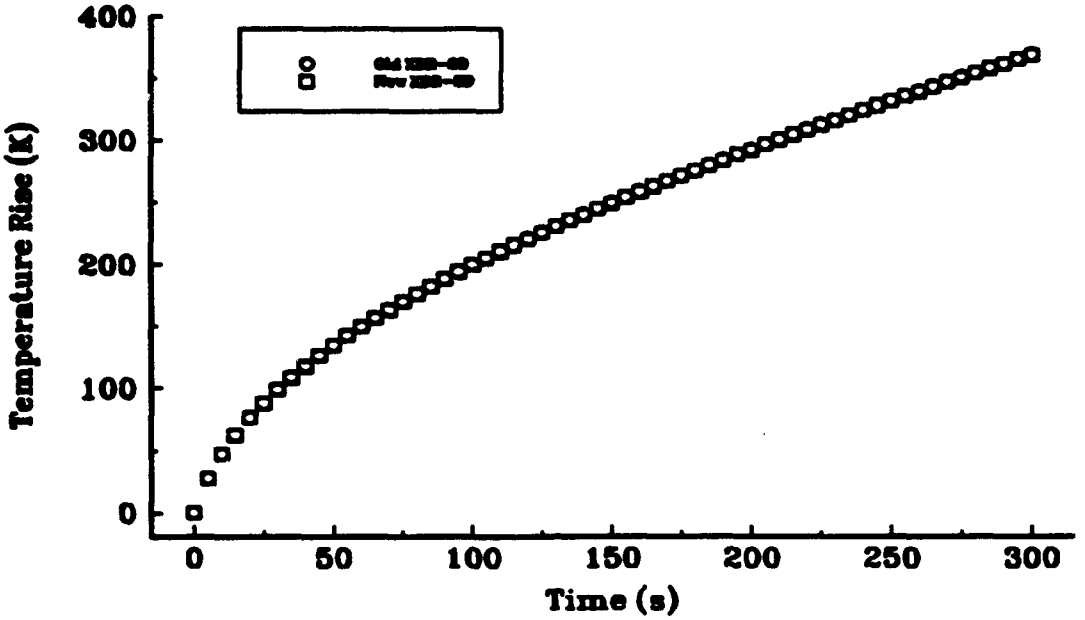

Figure 10. Residual temperatures at 10 in and a probe depth of 0.05 in for the 60-shot simulation.

4.2 120-mm Tank Gun. A test case modeling a 120-mm tank gun was assembled by Veritay. A three-shot burst of M829 tank rounds was modeled with a 10-s dwell time. The peak surface temperatures are summarized in Table 4. Figure 11 shows the surface temperature rise for the third shot of the burst. The new values were obtained after the code corrections described in Appendix C were implemented.

4.3 76-mm Cannon. A test case modeling a 76-mm Oto Melara gun was assembled by Veritay. This simulation, summarized in Table 5, included a three-round burst firing with a 1-s dwell time between shots. In this case, the new XBR-2D simulation was four times faster than the original XBR-2D simulation. Figure 12 compares the surface temperature history at the 22-in location and includes a magnified view of the third temperature peak. The pointed shape in the "old-XBR" curve is a result of plotting only every tenth point. The new values were obtained after the code corrections described in Appendix C were implemented.

Table 4. Comparison of Old and New XBR-2D Surface Temperature Rise for a Single-Shot 120-mm Test Case

Run	Execution Time (s)	Surface temperature rise (K) at each location. Locations in inches from the breech end.							
		15	20	25	30	35	40	45	50
Orig.	15,939	1,032.8	1,119.1	1,206.8	1,400.6	1,350.7	1,312.4	1,305.2	1,294.0
New	1,647	1,031.7	1,119.0	1,208.1	1,408.6	1,358.4	1,325.5	1,321.6	1,312.7

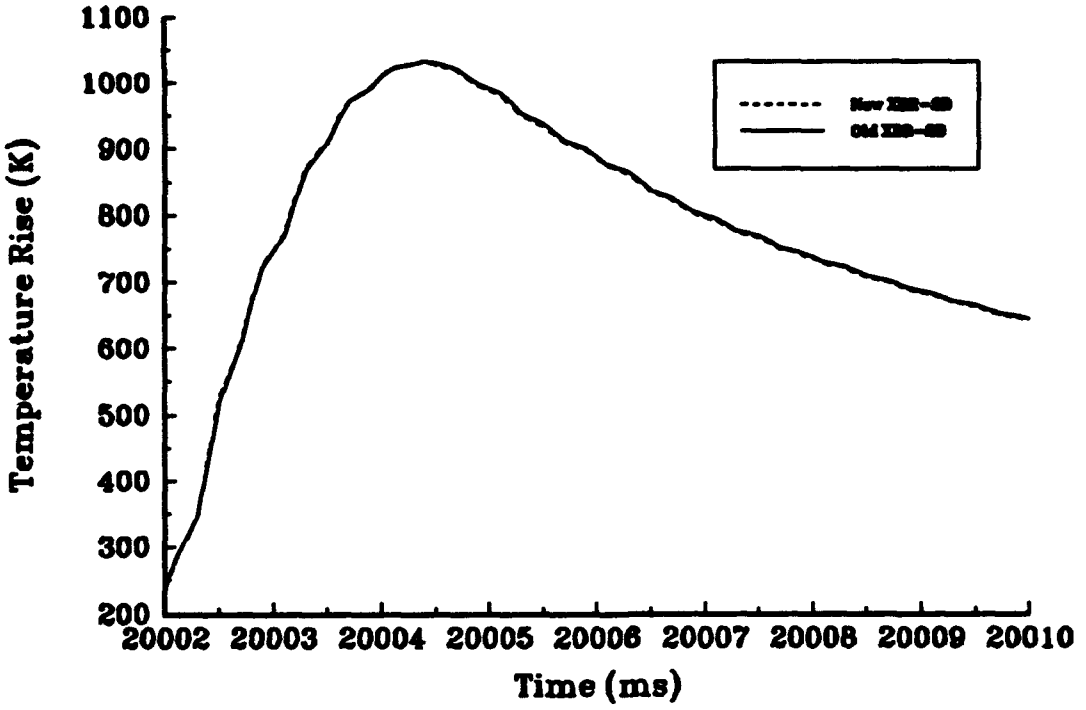

Figure 11. Surface temperatures at the 15-in location for the 120-mm gun simulations.

Table 5. Comparison of Old and New XBR-2D Surface Temperature Rise for a Single-Shot 76-mm Test Case

Run	Execution Time (s)	Peak surface temperature rise (K) at each location. Locations in inches from the breech end.					
		22.0	30.0	40.0	50.0	60.0	70.0
Orig.	4,452	883.4	865.5	746.5	611.4	510.3	539.8
New	1,158	864.9	871.2	762.6	631.9	525.2	560.4

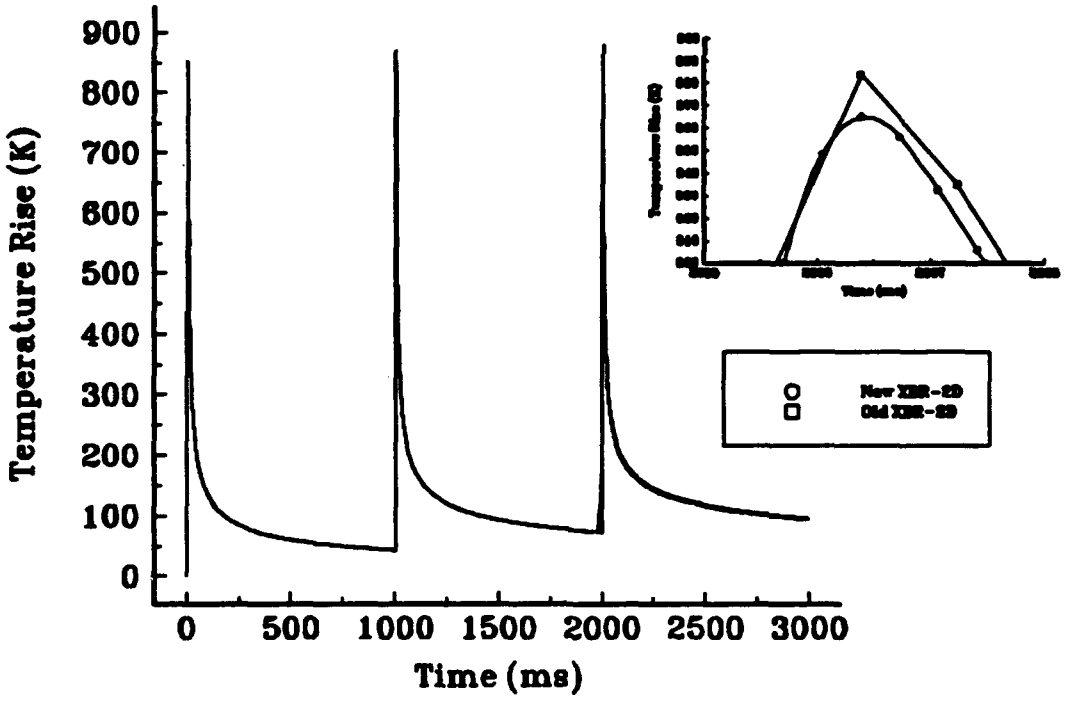

Figure 12. Surface temperature history at the 22-in location for the 76-mm gun simulation.

5. CONCLUSIONS AND RECOMMENDATIONS

The XBR-2D code was modified and execution time was decreased by a factor of 5.2 in the 155-mm howitzer sample case provided by the ARL. The decrease in execution time was mostly obtained by modulating the time step during the dwell period between shots. The longer the dwell period relative to the ballistic cycle, the greater the speed improvement will be. Several programming optimizations provided additional increases in efficiency and speed.

Techniques for adapting BEMs to gun barrel heating problems were explored. The method was used for a steady-state heat conduction problem and it appears very promising for both its accuracy and its speed. The formulation of a transient heat transfer BEM is a very complex process, and the limited scope of this effort did not allow this work to be completed. The theoretical background was developed to implement this mathematical technique in solving the 2-D, axisymmetric barrel heating problem; however, several obstacles remain that prevented its adoption in this program.

The Army may wish to consider funding an additional effort to incorporate this state-of-the-art numerical method. This effort would include development of approximation functions required to optimize the BEM technique for the transient barrel heating problem, and permit evaluation of the technique in terms of computational accuracy and speed. Another item that would improve the accuracy of the computed results is the inclusion of temperature-dependent material properties. At present, thermal diffusivity and thermal conductivity are treated as constant values in the formulation and integration of the governing equations.

6. REFERENCES

Anderson, D. A., J. C. Tannehill, and R. H. Pletcher. Computational Fluid Mechanics and Heat Transfer. New York: McGraw-Hill, 1984.

Becker, A. A. The Boundary Element Method in Engineering. New York: McGraw-Hill, pp. 238–245, 1992.

Brebbia, C. A., and J. Dominguez. Boundary Elements an Introductory Course. New York: McGraw-Hill, 1989.

Brebbia, C. A., and S. Walker. Boundary Element Techniques in Engineering. London: Newnes-Butterworths, 1980.

Carslaw, H. S., and J. C. Jaeger. Conduction of Heat in Solids. 1st ed., Oxford: Clarendon Press, pp. 291–319, 1948.

Chandra, S. Thermal Response Management of Barrels with XBR-2D. Final Report, Contract No. DAAA15-88-D-0014, U.S. Army Ballistics Research Laboratory, Aberdeen Proving Ground, MD, December 1990.

Curran, D. A. S., B. A. Lewis and M. Cross. "Solution of Parabolic Differential Equations by the Boundary Element Method Using Discretization in Time." Applied Mathematics Modeling, vol. 4, pp. 398–400, 1980.

Curran, D. A. S., B. A. Lewis, and M. Cross. "A Boundary Element Method for the Solution of the Transient Diffusion Equation in Two Dimensions." Applied Mathematics Modeling, vol. 10, pp. 107–113, 1986.

DeFigueiredo, D. B., and C. A. Brebbia. "Modelling Radiation Effects in BEM Using Nonlinear Conditions." Boundary Elements X, vol. 2, edited by C. A. Brebbia, New York: Springer-Verlag, pp. 223–231, 1988.

Morse, P. M., and H. Feshbach. Methods of Theoretical Physics. New York: McGraw Hill, vol. 1, pp. 791–895, 1953.

Onishi, K., and T. Kuroki. "Boundary Element Method in Singular and Nonlinear Heat Transfer." Boundary Element Methods in Engineering, edited by C. A. Brebbia, New York: Springer-Verlag, pp. 141–155, 1982.

Press, W. H., B. P. Flannery, S. A. Teukolsky, and W. T. Vetterling. Numerical Recipes. New York: Cambridge Press, 1989.

Rizzo, F. J., and D. J. Shippy. "A Method of Solution for Certain Problems of Transient Heat Conduction," AIAA Journal, vol. 8, pp. 2004–2009, 1990.

Wrobel, L. C. "On the Use of Time Dependent Fundamental Solutions for the Boundary Element Formulation of Diffusion Problems." Boundary Elements X. Vol. 2, Heat Transfer, Fluid Flow and Electrical Applications, edited by C. A. Brebbia, New York: Springer-Verlag, pp. 3–13, 1988.

Wrobel, L. C., C. A. Brebbia, and D. Nardini. "The Dual Reciprocity Boundary Element Formulation for Transient Heat Conduction." Finite Elements in Water Resources, vol. VI, edited by A. Sada Costa, et al., Berlin: Springer-Verlag, 1986.

Wrobel, L. C., J. C. F. Telles, and C. A. Brebbia. "A Dual Reciprocity Boundary Element Formulation for Axisymmetric Diffusion Problems." Boundary Elements VIII, vol. 1, edited by M. Tamaka and C. A. Brebbia, New York: Springer-Verlag, pp. 59–69, 1986.

APPENDIX A:

BOUNDARY ELEMENT METHOD

INTENTIONALLY LEFT BLANK.

BACKGROUND

The boundary element method (BEM) has received considerable attention over the past 15 years, and appears to hold much promise for use in solving transient heat conduction problems, although certain difficulties remain to be solved.

The BEM apparently originated as a scheme for numerical computations largely as an extension of approximation techniques involving Green's functions, integral equations, finite element schemes, and finite difference approaches (Brebbia and Walker 1980). The initial applications of BEM were directed toward time-independent spatial problems, such as steady-state heat flow, potential, and elastostatic problems. The application to time-dependent fields, including transient heating, has required additional attention to determine effective means of dealing with the time-dependence feature. This activity is still on-going.

A number of different BEM formulations have been advanced for treating transient heat conduction problems. The most successful from the standpoint of accuracy is, according to Wrobel (1988), the one which employs time-dependent fundamental solutions*. This approach is a numerical extension of the classical Green's function method (Morse and Feshbach 1953; Carslaw and Jaeger 1948) for obtaining analytical solutions to simple, tractable diffusion problems. Since no method has yet been found to completely separate the time dependence explicitly from the unknowns in the BEM equations (even when the time-dependent fundamental solution is used), it is still necessary to use a time marching scheme of some type to obtain a numerical solution of the BEM equations.

Two such time marching schemes have typically been used. In the first, the total time is divided into steps with each new step treated as a new problem. Within the initial time step the initial and boundary conditions can be used to solve the problem for the unknown variables. The temperatures at a number of points within the domain are calculated and used as initial values for the second time step, together with the original boundary values, to solve the problem anew for the second time interval. This process is repeated step by step until the final time is reached. The solution may become unstable if the time steps are very small (Becker 1992).

---

*The terminology "fundamental solution," referring to the governing partial differential equation, is a solution obtained for the infinite domain without taking into consideration specific finite boundary conditions of the problem.

In the second marching scheme, the integrations with respect to time always start from the initial conditions and the effect of the time evolution of heat transferred is determined through boundary integrations, so that values of temperature at points within the domain of interest are not required. However, the solution at any time step is still dependent on the solution at all previous time steps (not just the previous one as in the first marching scheme) going back to the initial time. This process suffers from requirements for large amounts of computation time and storage space (Becker 1992).

From a computational standpoint, these approaches using the time-dependent fundamental solution are recognized as having significant limitations (Wrobel 1988).

Alternate BEM formulations of the transient heat conduction problems include the use of Laplace transforms to remove the time dependency, solve the equations, and then apply the inverse Laplace transform to obtain physical values (Brebbia and Walker 1980; Rizzo and Shippy 1990). Another involves a coupled boundary element-finite difference (BE-FD) approach in which finite difference time steps are used (Curran, Lewis, and Cross 1980). This coupled scheme is similar to the first time marching scheme noted above. A third approach uses a potential-type method. This is an indirect version of the time-dependent Green's function method (Curran, Lewis, and Cross 1986). Several other approaches are also known (Wrobel 1988).

In recent years, there has been a trend towards the use of time-independent fundamental solutions together with an approximate treatment of the time derivative term. Two key references for this approach include the works of Wrobel, Brebbia, and Nardini (1986), and Wrobel, Telles and Brebbia (1986). Claims of significant reductions in computation time and storage requirements have been made when using this approach (Wrobel 1988; Wrobel, Telles, and Brebbia 1986).

Although a number of other BEM formulations were examined, efforts here emphasized this time-independent fundamental solution approach. The mathematical formulation of this BEM approach is summarized in the following section.

TIME-INDEPENDENT FUNDAMENTAL SOLUTION BEM FORMULATION

The transient heat equation to be solved for the temperature distribution $u(x,t)$ over the domain Ω is

$$\nabla^2 u\,(x,t) = \frac{1}{\kappa}\,\frac{\partial u}{\partial t}\,(x,t) \quad , \tag{A-1}$$

where x is a field point* with coordinates (x_1, x_2, x_3) in Ω or on its boundary Γ, and κ is a (constant) diffusivity coefficient.

Boundary conditions are taken here to be of the simple form

$$\begin{aligned} u(x) &= \bar{u}(x) && \text{on } \Gamma_1 \quad , \\ q(x) &= k\,\frac{\partial u(x)}{\partial n(x)} = \bar{q}(x) && \text{on } \Gamma_2 \quad , \end{aligned} \tag{A-2}$$

where $\Gamma = \Gamma_1 + \Gamma_2$ is the complete boundary of Ω, $q(x)$ is the flux, $n(x)$ is the unit outward normal at point x, and k is the (constant) thermal conductivity coefficient. These boundary conditions have been extended to include radiation effects by DeFigueiredo and Brebbia (1988) and Onishi and Kuroki (1982).

The initial condition at time $t = 0$ is of the form

$$u(x,o) = u_o(x) \qquad \text{on } \Omega \quad . \tag{A-3}$$

Now apply Green's second identity to a pair of the functions u and u*, where u* is the fundamental solution to Laplace's equation (not the transient heat equation)

$$k\,\nabla^2 u^*\,(\zeta, x) = -\,\delta^1\,(\zeta, x) \quad , \tag{A-4}$$

---

*The term "field point" in the current BEM literature refers to a general variable point, whereas "source point" (to be introduced in the following) is taken to be a fixed point for any one calculation.

and where $\delta^i(\xi,x)$ is the Dirac delta function. The function u represents the field generated by a concentrated unit source acting at point ξ. This gives as a result

$$\int_{\Omega}(u^{*}k\nabla^2 u - uk\nabla^2 u^{*})\,d\Omega = \int_{\Gamma}(u^{*}q - q^{*}u)\,d\Gamma \quad , \tag{A-5}$$

where

$$q^{*}(\zeta, x) = \frac{k\partial u(\zeta, x)}{\partial n(x)} \quad . \tag{A-6}$$

Recall that in equation A-5, u and q are functions of x, u^* and q^* are functions of ξ and x, and the integrations are carried out with respect to the variable x.

Substituting equation A-4 into A-5 gives the result

$$\int_{\Omega} u^{*}k\nabla^2 u\,d\Omega = -u^{i} + \int_{\Gamma}(u^{*}q - q^{*}u)\,d\Gamma \quad , \tag{A-7}$$

where u^i is the value of u at the source point ξ. For any other fixed position of the unit source i which might be chosen, the corresponding values of u^* and q^* will be different, and a new integral equation (of identical form) will apply.

The fundamental solution of equation A-4 for an isotropic three-dimensional (3-D) domain is

$$u^{*} = \frac{1}{4\pi r} \quad , \tag{A-8}$$

and for a two-dimensional (2-D) domain is

$$u^{*} = \frac{1}{2\pi}\ln\left(\frac{1}{r}\right) \quad , \tag{A-9}$$

where r is the distance from the unit point source at ξ to any other point under consideration.

Equation A-7 is valid for any fixed point ξ in the domain, but to formulate the problem as a boundary technique, the point ξ must be taken to the boundary. Upon accounting for this, and for the jump of the integral in q^*, the following integral equation is obtained (Wrobel, Telles, and Brebbia 1986):

$$\int_{\Omega} u^* k \nabla^2 u \, d\Omega = - c^i u^i + \int_{\Gamma} (u^* q - q^* u) \, d\Gamma \qquad \text{(A-10)}$$

where c^i is a function of the solid angle the boundary makes at a point ξ (see Brebbia and Dominguez 1989, p. 70), and the integral in q^* is calculated in the Cauchy principle value sense.

In the 2-D case, for example, if the boundary is smooth at the point ξ (i.e., there is no discontinuity of slope), the value of c^i is ½ rather than unity when ξ is an interior point. If a discontinuity of slope occurs at ξ then $c^i = \theta/2\pi$, where θ is the internal angle of the boundary Γ at ξ. The quantity c^i applies to the continuous boundary, as well as to the points where elements of the boundary join when the boundary is divided into a finite number of elements for numerical analysis.

Further, substituting equation A-1 into equation A-10 gives

$$\frac{k}{\kappa} \int_{\Omega} u^* \dot{u} \, d\Omega = - c^i u^i + \int_{\Gamma} u^* q d\Gamma - \int_{\Gamma} q^* u d\Gamma \qquad \text{(A-12)}$$

where

$$\dot{u} = \frac{\partial u}{\partial t} \quad .$$

Equation A-12 is the starting point for formulations which employ time-independent fundamental solutions. The treatment of the transient term on the left hand side of this equation differs in the schemes proposed in the literature (Wrobel, Telles, and Brebbia 1986).

STEADY-STATE SOLUTION PROCEDURE

To illustrate the procedure for obtaining a solution to equation A-12 over the boundary, consider first the simple steady-state case in which $\dot{u} = 0$. The integral term on the left-hand side of equation A-12 becomes zero and the following equation results:

$$c^i u^i + \int_{\Gamma} u q^* d\Gamma = \int_{\Gamma} u^* q d\Gamma \quad . \qquad \text{(A-13)}$$

Suppose the boundary is 2-D, smooth, and divided into N elements by a series of straight line segments whose ends lie on the boundary curve, and successively join one another to form a closed circuit about the boundary. The points at the middle of each element where unknown values (in equation A-13) are considered are called "nodes." Boundary elements of this type are called "constant" elements.

In this case of constant elements, the values of u and q are assumed to be constant over each element and equal to the value at the mid-element node. Equation A-13 can be discretized for a given point "i" before applying any boundary conditions as

$$\frac{1}{2}u^i + \sum_{j=1}^{N} \int_{\Gamma_j} uq^* d\Gamma = \sum_{j=1}^{N} \int_{\Gamma_j} qu^* d\Gamma \qquad \text{(A-14)}$$

where the point "i" is one of the boundary nodes and Γ_j is the boundary of the "j" element. For this type of element (i.e., constant) the boundary is always smooth, since the node is at the center of the element. Hence $c^i = ½$.

The u and q values can be taken out of the integrals since they are constant over each element. They are labelled u^j and q^j for each element "j," so equation A-14 becomes

$$\frac{1}{2}u^i + \sum_{j=1}^{N} \left(\int_{\Gamma_j} q^* d\Gamma \right) u^j = \sum_{j=1}^{N} \left(\int_{\Gamma_j} u^* d\Gamma \right) q^j$$

or

$$\frac{1}{2}u^i + \sum_{j=1}^{N} \hat{H}^{ij} u^j = \sum_{j=1}^{N} G^{ij} q^j \quad , \qquad \text{(A-15)}$$

where

$$\hat{H}^{ij} = \int_{\Gamma_j} q^* d\Gamma \; , \; G^{ij} = \int_{\Gamma_j} u^* d\Gamma \quad . \qquad \text{(A-16)}$$

These integrals relate the "i" node where the fundamental solution is acting to any other node "j."

If it is assumed that the position i can also vary from 1 to N, corresponding to an application of the fundamental solution at each node successively, then one obtains a system of equations resulting from applying equation A-15 to each boundary point.

Further, if one lets

$$H^{ij} = \begin{cases} \hat{H}^{ij} & \text{when } i \neq j \\ \hat{H}^{ij} + \dfrac{1}{2} & \text{when } i = j \end{cases}, \tag{A-17}$$

then equation A-16 can be written as

$$\sum_{j=1}^{N} H^{ij} u^j = \sum_{j=1}^{N} G^{ij} q^j . \tag{A-18}$$

This set of equations for the unknowns u^j and q^j can be written in matrix form as

$$\underline{H}\,\underline{U} = \underline{G}\,\underline{Q}, \tag{A-19}$$

where $\underline{H}$ and $\underline{G}$ are two $N \times N$ matrices, and $\underline{U}$, $\underline{Q}$ are vectors of length N.

Since there are N_1 values of u and N_2 values of q known on portions Γ_1 and Γ_2 respectively, where $N_1 + N_2 = N$, there are only N unknowns in the system of equations A-19. To introduce these known boundary values into equation A-19, the system must be rearranged by moving columns of $\underline{H}$ and $\underline{G}$ from one side to the other. When all the unknowns are passed to the left-hand side, the system can be written

$$A\,X = F \tag{A-20}$$

where $\underline{F}$ is a vector of unknown (u's and q's) boundary values.

Equation A-20 can be solved, and all the boundary values will then be known. With this information, any internal value of u or its derivatives can be calculated at any internal point "i" using the corresponding steady-state form of equation A-7,

$$u^i = \int_\Gamma q\,u^*\,d\Gamma - \int_\Gamma u\,q^*\,d\Gamma . \tag{A-21}$$

Here the fundamental solution is considered to be acting on an internal point "i," and all the values of u and q on the boundary are already known.

The process is then one of numerical integration. The same discretization is used for the boundary integrals

$$u^i = \sum_{j=1}^{N} G^{ij} q^j - \sum_{j=1}^{N} \hat{H}^{ij} u^j \,, \tag{A-22}$$

and the coefficients G^{ij} and $\hat{H}^{ij}$ must be calculated again for each different internal point i.

TIME INDEPENDENT FORMULATION

To proceed with the formulation of time-independent fundamental solutions using equation A-12, the so-called Dual Reciprocity BEM developed by Wrobel and co-workers (Wrobel 1988; Wrobel, Telles, and Brebbia 1986) will be outlined here.

The function $\dot{u}$ at any point inside the domain Ω is approximated by a set of N (chosen)* coordinate functions $f^j(x)$ multiplied by functions $\dot{\alpha}^j(t)$, which are unknowns,

$$\dot{u}(x,t) = \sum_{j=1}^{N} f^j(x)\, \dot{\alpha}^j(t) \,. \tag{A-23}$$

Using this approximation, the domain integral on the left-hand side of equation A-12 becomes

$$\int_\Omega u^* \dot{u}\, d\Omega = \sum_{j=1}^{N} \dot{\alpha}^j \int_\Omega f^j u^*\, d\Omega \quad . \tag{A-24}$$

It is further assumed that there exists a function $\psi^j(x)$ for each function $f^j(x)$, where the two functions are related by

$$\nabla^2 \psi^j(x) = f^j(x) \,. \tag{A-25}$$

Substituting equation A-25 into equation A-24 gives

$$\int_\Omega u^* \dot{u}\, d\Omega = \sum_{j=1}^{N} \dot{\alpha}^j \int_\Gamma \nabla^2 \psi^j u^*\, d\Omega \quad . \tag{A-26}$$

Introducing expression A-26 into equation A-12 yields the result

*Choosing the coordinate function f^i will be briefly addressed later.

$$c^i u^i + \int_\Gamma q^* u \, d\Gamma - \int_\Gamma u^* q \, d\Gamma = \sum_{j=1}^{N} \frac{1}{\kappa} \alpha^j \left\{ - \int_\Omega u^* k \nabla^2 \psi^j \, d\Omega \right\} . \qquad \text{(A-27)}$$

Now applying the transformation indicated in equation A-10 to the domain integral gives the result

$$c^i u^i + \int_\Gamma q^* u \, d\Gamma - \int_\Gamma u^* q \, d\Gamma = \sum_{j=1}^{N} \frac{1}{\kappa} \left\{ c^i \psi^{ij} + \int_\Gamma q^* \psi^j \, d\Gamma - \int_\Gamma u^* \eta^j \, d\Gamma \right\} \alpha^j \qquad \text{(A-28)}$$

where

$$\eta^j = k \frac{\partial \psi^j}{\partial n} .$$

Equation A-28 involves boundary integrals only.

Wrobel and co-workers (Wrobel 1988; Wrobel, Telles, and Brebbia 1986) found it convenient to approximate the variation of functions u, q, ψ, and η within each boundary element using a unique (unspecified) set of interpolation functions Φ, such that

$$u = \Phi^T u_e$$

$$q = \Phi^T q_e$$

$$\psi^j = \Phi^T \psi^j_e \qquad \text{(A-29)}$$

and

$$\eta^j = \Phi^T \eta^j_e$$

where subscript e denotes a particular boundary element.

Wrobel (1988) claims that it is not necessary to approximate the functions ψ and η this way over the boundary, since they are known once the set of functions f^j are chosen. However, he notes that this approximation dramatically reduces the required boundary integrations, with some sacrifice in accuracy. The seriousness of this sacrifice is unknown, but should be explored.

Upon dividing the boundary into elements, applying the discretized version of equation A-28 to each boundary node, and taking the preceding approximations into account, the following system of equations (written in matrix form) results:

$$H\,U - G\,Q = \frac{1}{\kappa}(H\,U\psi - G\,\eta)\,\dot{\alpha}\ . \tag{A-30}$$

By evaluating the discretized version of equation A-23 at all boundary nodes, one finds

$$\dot{U} = F\,\dot{\alpha}\ . \tag{A-31}$$

Upon inversion, this yields the result

$$\dot{\alpha} = F^{-1}\,\dot{U}\ . \tag{A-32}$$

Substituting expression A-32 into equation A-30 gives the matrix form

$$C\,\dot{U} + H\,U = G\,Q \tag{A-33}$$

where

$$C = \frac{-1}{\kappa}(H\,\psi - G\,\eta)F^{-1}\ .$$

In the matrix equation A-33, the vectors U and Q each have the dimension equal to the number N of boundary nodes, and the matrices C, H and G are of the size (i.e., $N \times N$) of standard boundary element matrices.

Wrobel and co-workers (Wrobel 1988; Wrobel, Telles, and Brebbia 1986) further utilized a simple, two-level time integration scheme in their work. This involved using a linear approximation for U and Q within each time step of the form

$$U = (1 - \beta)\,U^{m} + \beta U^{m+1}$$

$$Q = (1 - \beta)\,Q^{m} + \beta\,Q^{m+1}$$

$$\dot{U} = \frac{1}{\Delta t}(U^{m+1} - U^{m}) \tag{A-34}$$

where β ($0 \le \beta \le 1$) is a parameter which indicates the values of U and Q between time levels m and $m + 1$.

Substituting these approximations into equation A-33 results in the following

$$\left(\frac{1}{\Delta t}C + \beta H\right)U^{m+1} - \beta G Q^{m+1} = \left(\frac{1}{\Delta t}C - (1-\beta)H\right)U^{m} + (1-\beta) G Q^{m} . \qquad \text{(A-35)}$$

The right-hand side of equation A-35 is known at time m Δt. By introducing the boundary conditions at time (m + 1) Δt, the left-hand side of equation A-35 can be rearranged, and the system of equations can be solved for this time step.

SELECTION OF COORDINATE FUNCTIONS

The selection of coordinate functions $f^j(x)$ used to approximate the time derivative of the dependent variable u(x,t) over the domain Ω is apparently quite important. Certainly it needs further attention in any future effort to apply this overall BEM to the barrel heating problem.

Wrobel (1983) conjectures that the choice of functions, $f^j(x)$, should correspond to the behavior of the fundamental solution itself. He has apparently had some success in 2- and 3-D problems with Cartesian coordinates using functions of the form

$$f^j(x) = R(x, x^j) . \qquad \text{(A-36)}$$

Here R represents the Euclidean distance between two points in space, x^j are coordinates of the jth fixed point, and x are the coordinates of any point in the domain Ω. This set of coordinate functions is linearly independent as long as the fixed points are separate (not coincident). The corresponding functions ψ and η are

$$\psi^j(x) = \frac{1}{a} R^3(x, x^j) \qquad \text{(A-37)}$$

and

$$\eta^j(x) = \frac{3k}{a} R^2(x, x^j) \frac{\partial R}{\partial n} , \qquad \text{(A-38)}$$

where a has the value of 9 or 12 for 2- or 3-D problems, respectively.

For axisymmetric problems, Wrobel, Telles, and Brebbia (1986) have suggested the use of coordinate functions of the form

$$f^j(x)=R'(x,x^j)[1-\frac{r^j}{4r}] \ , \tag{A-39}$$

where r^j (or r) is the distance from a fixed point (or any point in the domain Ω) to the axis of revolution, and R' is the Euclidean distance between points defined in the (r,z) plane (i.e., on the generating plane θ = constant). In this case, the expressions for ψ and η are of the form

$$\psi^j(x)=\frac{1}{12}R'^3(x,x^j) \tag{A-40}$$

and

$$\eta^j(x)=\frac{k}{4}R'^2(x,x^j)\frac{\partial R}{\partial n} \ . \tag{A-41}$$

Wrobel (1988) also notes the following items:

(1) The functions f^j should be linearly independent for the matrix F to have an inverse.

(2) Once the family f^j is chosen, it is usually easy to determine the functions ψ^j and η^j.

(3) The position and number of fixed points is conveniently chosen to coincide with the boundary nodes.

(4) The inclusion of an internal point associated with f = constant may be required to better simulate the heating up of the entire body by a constant value.

APPENDIX B:
CORRECTIONS TO XBR-2D CODE

INTENTIONALLY LEFT BLANK.

There were two major errors in the original XBR-2D release that were discovered and pointed out to Veritay by Army Research Laboratory (ARL) personnel near the end of this effort. Figure B-1 illustrates the results from several runs with the original code. These curves represent the surface temperature rise at the 42-in location of a 155-mm howitzer. The only implicit input differences between the seven runs are the locations of the left and right hand computational boundaries. The resulting temperatures are very different from each other. It was this finding that called attention to the errors in coding.

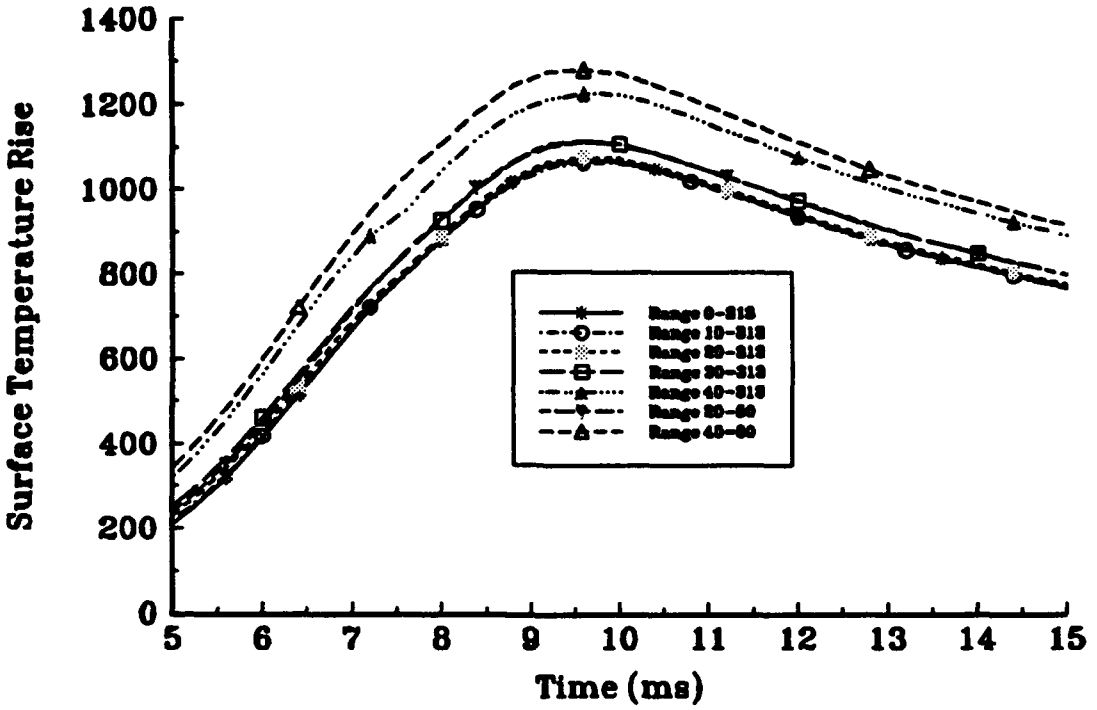

Figure B-1. Original XBR-2D runs with various computational regions.

One of the interpolation functions in the code, which converts the geometric parameters from the input file's axial positions to that of the individual grid locations, had a mistake in the formulation. The left side boundary was always assigned the geometric values of the first input value (inside and outside diameters), no matter where this boundary was located. If the left side boundary was not equal to the first geometric location in the input file, the wrong geometry was used for that point. This has been corrected in the new version of the code.

A more significant error present in the original code was the treatment of the thermal boundary layer. The thickness of the boundary layer was always set to zero at the left hand boundary. This is not correct

for a left side boundary that does not start at the rear of the gun. This error results in a much thinner thermal boundary layer than is correct if the left side boundary is not at the rear of the gun.

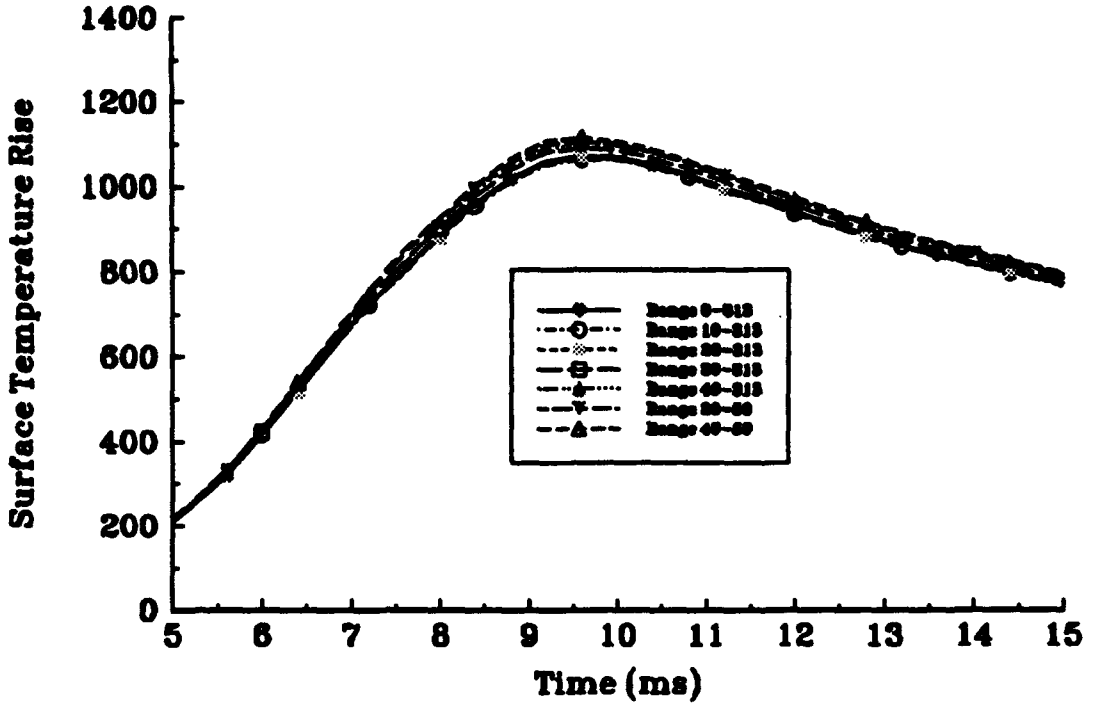

Figure B-2. Corrected XBR-2D runs with various computational regions.

This error was corrected by adding subroutine PZDZIN which calculates the thickness of the thermal boundary layer up to the left side boundary and uses this as an initial condition for the calculations. The test cases run in Figure B-1 were repeated after the corrections were made and are presented in Figure B-2.

The agreement between the curves is reasonable considering the wide range of spatial resolutions that are represented in the figure. The first curve defined the simulation's 100 grids to represent the entire barrel, thus forcing the axial grid spacing (Δz) to be 3.13 in. Conversely, the last simulation presented defines the code's 100 grids over a mere 10 in, making the axial spacing 0.1 in. For simulations conducted using previous versions of the XBR-2D code, the results will change slightly if the left computational boundary was not set to zero. Simulations with a left boundary at $z = 0$ should be essentially unchanged from the previous version of the code.

APPENDIX C:

FURTHER IMPROVEMENTS TO THE XBR-2D CODE

INTENTIONALLY LEFT BLANK.

The original XBR-2D code contained some errors in coding and in theory. These errors were corrected and implemented in version 1.20. The addition of multiple grids in the chrome layer, if that layer becomes thick, was also added as a new feature of version 1.20.

FINITE DIFFERENCE EQUATION

The original finite difference equation in XBR was correct if the geometric factor was constant throughout the thickness. However, the code, in fitting the gridding to the barrel geometry, modified the grids such that the geometric factor between the first and second grid was different from the geometric factor between the rest of the grids.

To correct this error and to accommodate the modification which allows for multiple grids through the chrome layer, the finite difference equation was modified to allow for a general gridding scheme with different radial grid spacing in either direction. The Δr is computed for each radial position and it is this value, not the geometric factor, which is used in the finite difference equation.

For the Fourier equation of heat conduction in cylindrical coordinates,

$$\frac{\delta^2 T}{\delta r^2} + \frac{1}{r}\frac{\delta T}{\delta r} + \frac{1}{A_z}\frac{\delta}{\delta z}\left(A_z \frac{\delta T}{\delta z}\right) = \frac{1}{\alpha}\frac{\delta T}{\delta t} . \qquad \text{(C-1)}$$

The generalized finite difference equation for variable Δr is:

$$\frac{1}{\alpha}\frac{\Delta T_{ij}}{\Delta t} = \frac{2}{\left(\Delta r_+^2 + \Delta r_-^2\right)}\left[T_{ij+1} - 2T_{ij} + T_{ij-1} - \frac{\left(\Delta r_+ - \Delta r_-\right)}{\left(\Delta r_+ + \Delta r_-\right)}\left[T_{ij+1} - T_{ij-1}\right]\right]$$

$$+ \frac{1}{r_{ij}\left(\Delta r_+ + \Delta r_-\right)}\left[T_{ij+1} - T_{ij-1}\right] + \frac{1}{\Delta z^2}\left[T_{i-1j} - 2T_{ij} + T_{i+1j}\right]$$

$$+ \frac{1}{A_z 2\Delta z}\left[T_{i-1j} + T_{i+1j}\right]\frac{1}{2\Delta z}\left[A_{i+1j} + A_{i-1j}\right] . \qquad \text{(C-2)}$$

The generalized finite difference equation for variable Δr at the chrome-steel interface is:

$$\frac{\Delta T_{ij}}{\Delta t} = \frac{2}{\left(\Delta r^2_+ + \Delta r^2_-\right)}\left[\alpha_e T_{ij+1} - 2\alpha_{ave} T_{ij} + \alpha_e T_{ij-1} - \frac{\alpha_{ave}\left(\Delta r_+ - \Delta r_-\right)}{\left(\Delta r_+ + \Delta r_-\right)}\left[T_{ij+1} - T_{ij-1}\right]\right]$$

$$+ \frac{1}{r_{ij}\left(\Delta r_+ + \Delta r_-\right)}\left[\alpha_e T_{ij+1} - \alpha_e T_{ij-1}\right] + \frac{\alpha_{ave}}{\Delta z^2}\left[T_{i-1j} - 2T_{ij} + T_{i+1j}\right]$$

$$+ \frac{\alpha_{ave}}{A_i 2\Delta z}\left[T_{i-1j} + T_{i+1j}\right]\frac{1}{2\Delta z}\left[A_{i+1j} + A_{i-1j}\right] . \qquad \text{(C-3)}$$

These two equations were implemented in XBR version 1.20 to replace the original finite difference equations.

RADIAL GRIDDING

In the original versions of XBR-2D, the number of radial grids was computed based on the local thickness. This could result in, for certain geometries, different numbers of radial grids as the thickness varied axially. In such a situation, the axial heat conduction calculations were invalid. This was corrected by computing the number of grids required for the thinnest part of the barrel and stretching that number of grids to fit the thickness at other axial positions.

Two other alternatives were tested: (1) basing the number of grids on the thickest part of the barrel and shrinking the grids to fit into the thinner parts, and (2) using an average thickness and both shrinking and stretching, where appropriate, to fit the barrel geometry. Both of these methods caused the grid sizes to become extremely small in the thinnest section of the barrel when grid shrinking was resolved. This resulted in a drastic reduction in the time step and a correspondingly large increase in execution time.

MULTIPLE GRIDS IN THE CHROME LAYER

XBR-2D originally fixed the thickness of the first grid to the thickness of the chrome layer, if such a layer was present. If the chrome layer becomes thick, or XBR is used to model other types of liners,

the chrome layer must be modeled with more than one grid. XBR was modified so that, if a chrome layer is present, the first grid's thickness is based on the time step. If the chrome thickness is greater than this thickness, then the thickness of the second grid is computed based on the geometric factor and this process is continued until the chrome thickness is reached. The exact thickness of the chrome is then accomplished by shrinking the grids to this thickness. The interface between the chrome and steel is handled by Equation 2.

THERMAL BOUNDARY LAYER

The thermal boundary layer is calculated using the method described by Stratford and Beavers (S&B) in 1961. In the translation from the paper to the code several mistakes were made. The code originally had the Mach number weighting function, P_z, defined as:

$$P_z = M^4 \left[1 - \frac{1}{2}(\gamma - 1) M^2\right]^{\frac{3\gamma-1}{2(\gamma-1)}} . \qquad \text{(C-4)}$$

After reviewing the S&B method, it was determined that the equation for the Mach number weighting function should be:

$$P_z = \left(\left[\frac{M}{1 + \frac{1}{2}(\gamma - 1)M^2}\right]^{\frac{3\gamma-1}{2(\gamma-1)}}\right) r^{1.25} . \qquad \text{(C-5)}$$

The term $r^{1.25}$ was S&B's correction for axisymmetric flow. The other corrections involved moving the Mach number inside the brackets and correcting and moving the second term to the denominator of the expression. This corrected equation now agrees with the method described by S&B in their 1961 paper.

MODIFICATIONS TO THE RESTART OPTION

The original coding of the restart option required the simulation, when restarted, be run with the same configuration and timing as the original run. This was slightly modified in the new version of the code. The code now writes the time into the file LASTTEMP.OUT. When the restart option is chosen, the simulation uses this time as the starting point. This allows simulations of various firing rates to be run.

NEW INPUT FILE FORMAT

Two more output flags were added to the input file for graphical output files, and an additional line was added where the barrel and chrome material properties must be input. Following is a sample input file

```
;;-------------------------------------------------------------------------
;;    Sample XNR-2D input file for a 25-mm Barrel  (750 Shots/min)
;;-------------------------------------------------------------------------
;
; Ambient Temp (R), Pr (psi), gas vel (in/s)
;  :    ..............:            :
;  :    :    ........................:
;  :    :    :

530.0 14.70 0.00

;
; Barrel Geometry :
;-------------------------------------------------------------------------
; xchrom (in), tmaxv (ms), xcon, xcham (in), zmax (in)
;  :     .........:         :      :          :
;  :     :     ..............:      :          :
;  :     :     :      ..............:          :
;  :     :     :      :                       :
;  :     :     :      :     ...................:
;  :     :     :      :     :    nloc , zstart (in), zend (in)
;  :     :     :      :     :     :         :          :
;  :     :     :      :     :     :    .....:          :
;  :     :     :      :     :     :    :    ...........:
;  :     :     :      :     :     :    :    :

0.005  4080.0 0.100  4.60 73.5   20  0.0   10.0

;
; ndtz, zdb (1:ndtz) -- no of axial locations, ndtz locations (in)
; (max = 8)
;
;   1    2     3     4     5     6     7     8
;

7  0.0  4.0  13.0   23.0  43.0  65.0  75.0

;
; dbar (1:ndtz)      -- barrel o.d. at ndtz locations (in)
;
;   1     2     3     4     5    6     7     8
;

  2.75  2.75  2.25  2.00  1.90  1.75  1.65

;
; dbor (1:ndtz)      -- barrel i.d. at ndtz locations (in)
;
;   1     2     3     4     5    6     7     8
;
```

```
  1.024 1.024 1.024 1.024 1.024 1.024 1.024

;
; Desired Output Locations:
;-------------------------------------------------------------------------
; nhtz, zout (1:nhtz)-- no of locations for output, nhtz locations (in)
; (max -8)
;
;   1     2     3     4     5     6     7     8
;

8  4.625 4.625 4.625 4.625 7.0   7.0   7.0   7.0

;
; rout (1:nhtz)       -- radial depth at nhtz locations (in)
;
;   1     2     3     4     5     6     7     8
;

   0.0  0.005  0.025  0.5  0.0   0.005  0.02   .5

;
; Firing Data:
;-------------------------------------------------------------------------
; nrounds, nkount1, nkount2, deltv (s), lastshot
;   ..........:       :        :           :
;   :  .............:        :           :
;   :  :    .................:           :
;   :  :    :      ......................:
;   :  :    :      :

1 10 50 3.0D-5   1

;
; Desired Output Units and Files:
;-------------------------------------------------------------------------
; iunit (0 for K, 1 for deg R)
; ... itemp (0 for as calculated, 1 for temp rise),
; :
; :       iout (1:9) ---
; :
; : ............ screen output
; : : :
; : : : ............. single shot probe temperature,
; : : : : ............single shot inside surface temperature,
; : : : : : ..........single shot outside surface temperature,
; : : : : : :
; : : : : : .......... burst fire probe temperature,
; : : : : : : ........ burst fire inside surface temperature,
; : : : : : : : ...... burst fire outside surface temperature,
; : : : : : : : :
; : : : : : : : : ....... heat transfer coefficient,
; : : : : : : : : : ..... effective gas temperature history
; : : : : : : : : : :

0 0 0 2 0 2 0 1 0 0 0 0 0

;                     : :
;                     : . ..... graphical output file
```

```
;                        :..... graphical output file
;
;
; Barrel   Barrel     Chrome    Chrome
;   k        α          k         α

4.6482    0.0156     8.3595    0.03131
```

TESTS PERFORMED ON XBR-2D VERSION 1.20

Test No. 1: Using steel plating on a steel barrel, vary the plating thickness and see if the results are consistent.

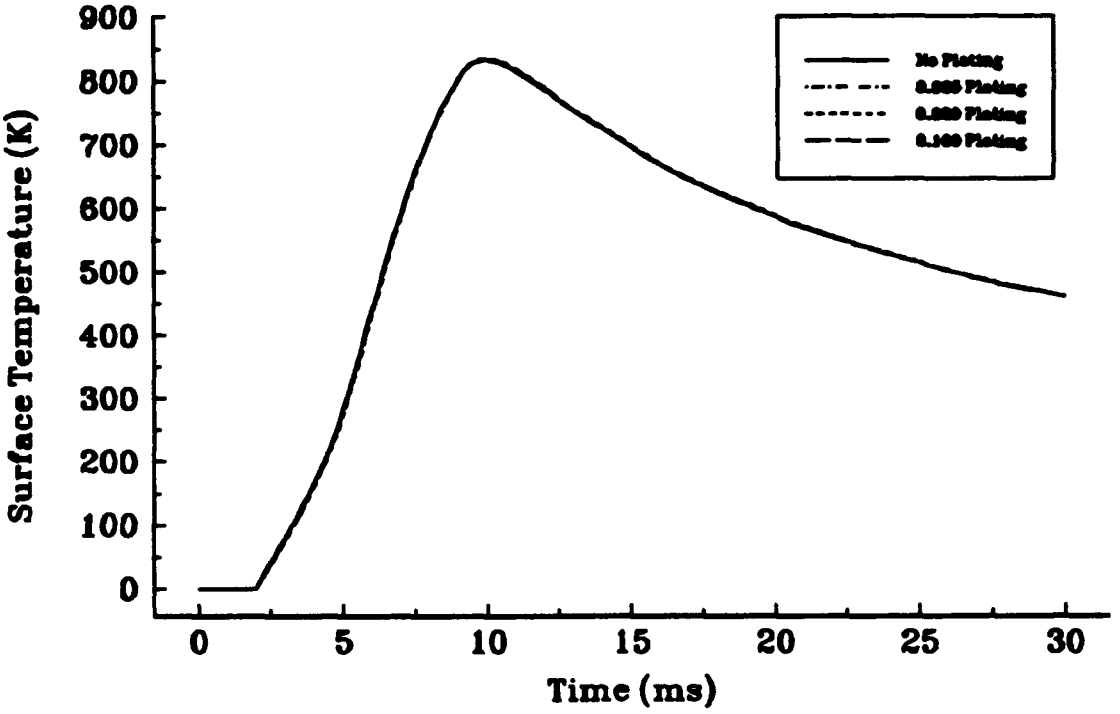

Figure C-1. 155-mm howitzer test case with various steel plating thicknesses.

Test No. 2: Vary the geometric factor from 0.1 to 0.3 and observe the temperature.

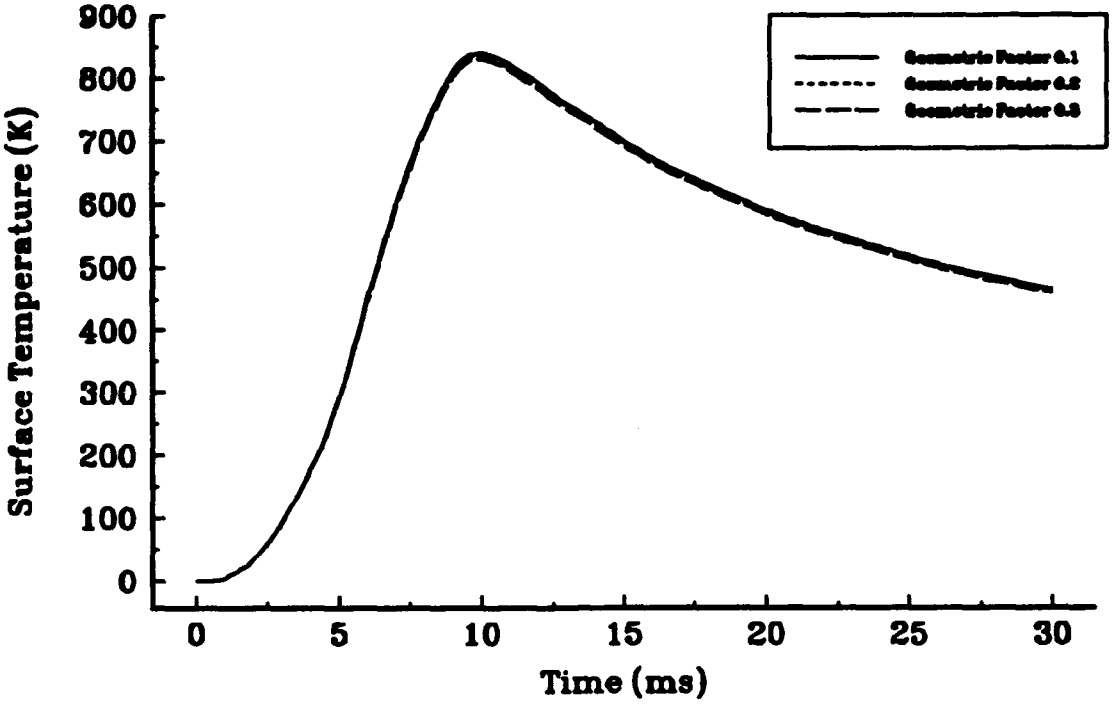

Figure C-2. Variation of geometric factors in a 155-mm howitzer.

Test No. 3: Examine the thickness of the boundary layer in detail vs. both time and position.

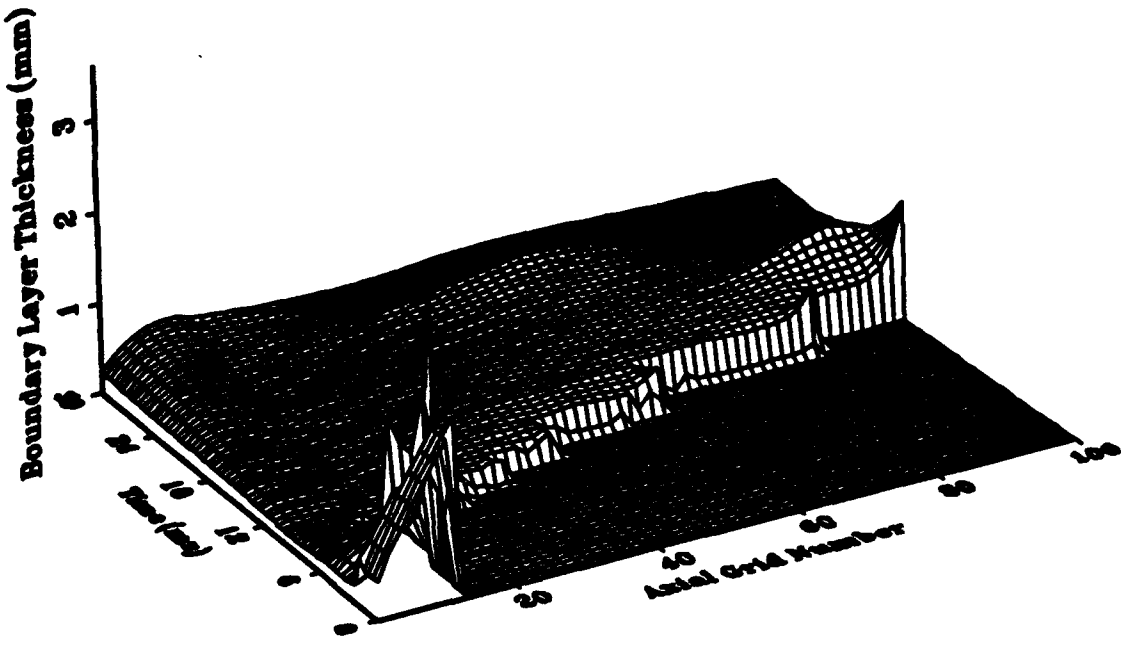

Figure C-3. Thickness of the thermal boundary layer predicted by Stratford and Beavers vs. time and position in a 155-mm howitzer.

Test No. 4: Examine the Mach number profile down the barrel.

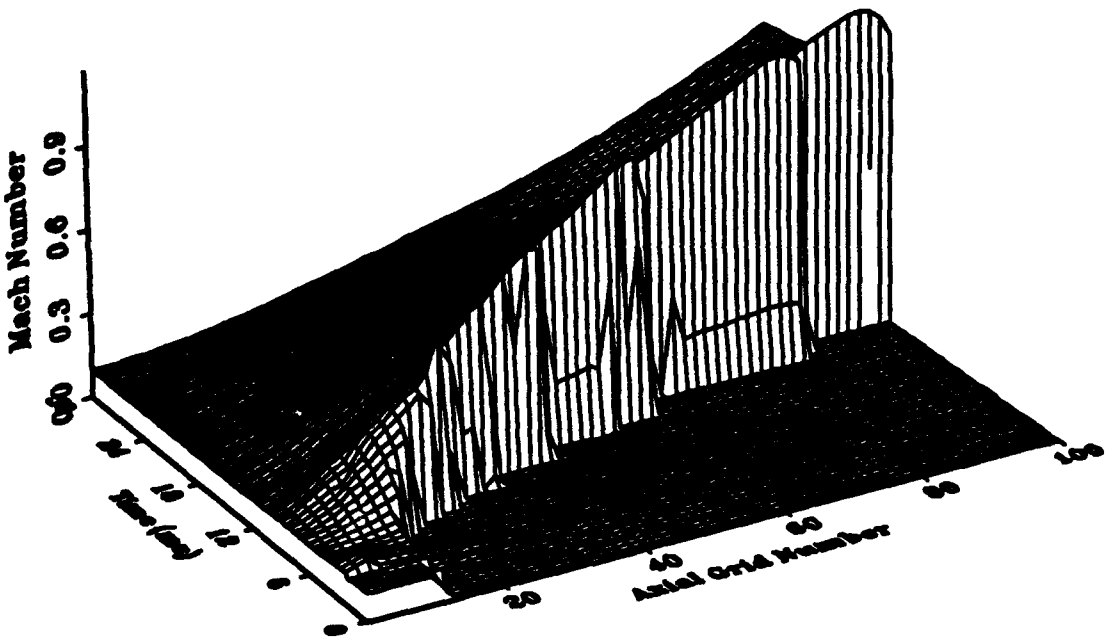

Figure C-4. Mach number profiles vs time and position for the 155-mm howitzer test case.

Test No. 5: Apply a constant heat flux to the bore surface and compare the results to an analytical solution.

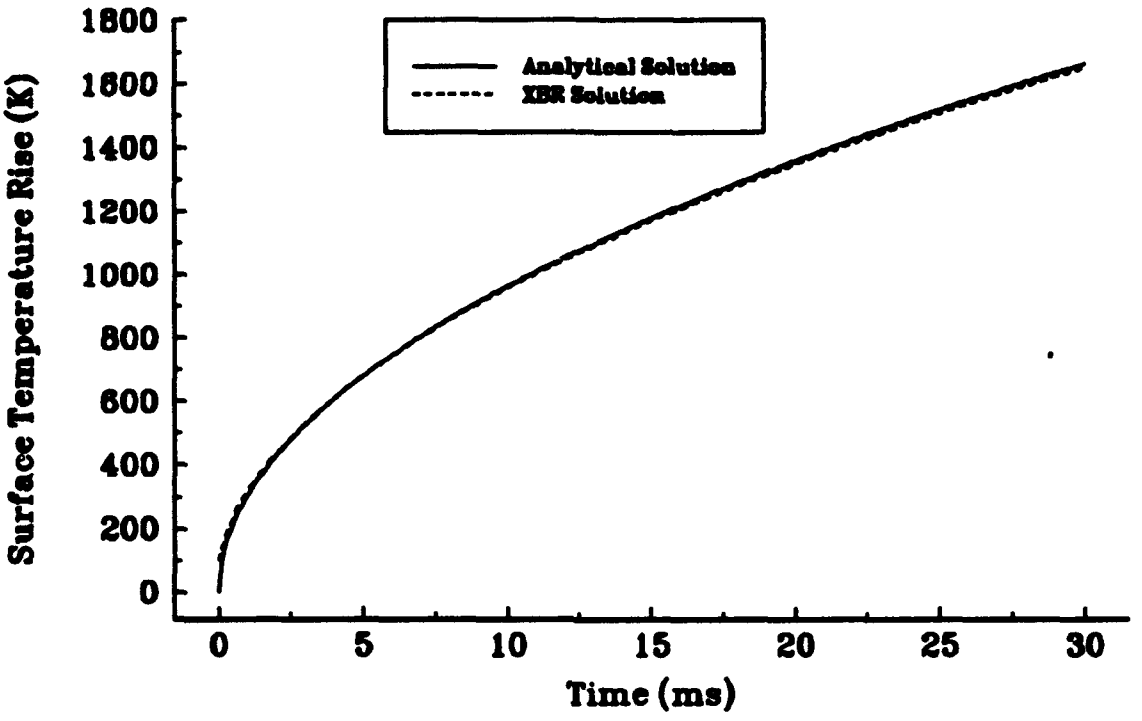

Figure C-5. Comparison of XBR with a constant heat flux to an analytical solution.

A heat flux of 1,000,000 watts was applied to the surface. The analytical solution was obtained from the equation:

$$T(x,t) = T_i + \frac{2q''\sqrt{\frac{\alpha t}{\pi}}}{k}.$$

INTENTIONALLY LEFT BLANK.

No. of Copies	Organization
2	Administrator Defense Technical Info Center ATTN: DTIC-DDA Cameron Station Alexandria, VA 22304-6145
1	Commander U.S. Army Materiel Command ATTN: AMCAM 5001 Eisenhower Ave. Alexandria, VA 22333-0001
1	Director U.S. Army Research Laboratory ATTN: AMSRL-OP-CI-AD, Tech Publishing 2800 Powder Mill Rd. Adelphi, MD 20783-1145
1	Director U.S. Army Research Laboratory ATTN: AMSRL-OP-CI-AD, Records Management 2800 Powder Mill Rd. Adelphi, MD 20783-1145
2	Commander U.S. Army Armament Research, Development, and Engineering Center ATTN: SMCAR-TDC Picatinny Arsenal, NJ 07806-5000
1	Director Benet Weapons Laboratory U.S. Army Armament Research, Development, and Engineering Center ATTN: SMCAR-CCB-TL Watervliet, NY 12189-4050
1	Director U.S. Army Advanced Systems Research and Analysis Office (ATCOM) ATTN: AMSAT-R-NR, M/S 219-1 Ames Research Center Moffett Field, CA 94035-1000

No. of Copies	Organization
1	Commander U.S. Army Missile Command ATTN: AMSMI-RD-CS-R (DOC) Redstone Arsenal, AL 35898-5010
1	Commander U.S. Army Tank-Automotive Command ATTN: AMSTA-JSK (Armor Eng. Br.) Warren, MI 48397-5000
1	Director U.S. Army TRADOC Analysis Command ATTN: ATRC-WSR White Sands Missile Range, NM 88002-5502
(Class. only) 1	Commandant U.S. Army Infantry School ATTN: ATSH-CD (Security Mgr.) Fort Benning, GA 31905-5660
(Unclass. only) 1	Commandant U.S. Army Infantry School ATTN: ATSH-WCB-O Fort Benning, GA 31905-5000
1	WL/MNOI Eglin AFB, FL 32542-5000
	Aberdeen Proving Ground
2	Dir, USAMSAA ATTN: AMXSY-D AMXSY-MP, H. Cohen
1	Cdr, USATECOM ATTN: AMSTE-TC
1	Dir, USAERDEC ATTN: SCBRD-RT
1	Cdr, USACBDCOM ATTN: AMSCB-CII
1	Dir, USARL ATTN: AMSRL-SL-I
5	Dir, USARL ATTN: AMSRL-OP-AP-L

No. of Copies	Organization
1	Chairman DOD Explosives Safety Board Room 856-C Hoffman Bldg. 1 2461 Eisenhower Avenue Alexandria, VA 22331-0600
1	Headquarters U.S. Army Materiel Command ATTN: AMCICP-AD, M. Fisette 5001 Eisenhower Ave. Alexandria, VA 22333-0001
1	U.S. Army Ballistic Missile Defense Systems Command Advanced Technology Center P.O. Box 1500 Huntsville, AL 35807-3801
1	Department of the Army Office of the Product Manager 155mm Howitzer, M109A6, Paladin ATTN: SFAE-AR-HIP-IP, Mr. R. De Kleine Picatinny Arsenal, NJ 07806-5000
3	Project Manager Advanced Field Artillery System ATTN: SFAE-ASM-AF-E, LTC A. Ellis T. Kuriata J. Shields Picatinny Arsenal, NJ 07801-5000
1	Project Manager Advanced Field Artillery System ATTN: SFAE-ASM-AF-Q, W. Warren Picatinny Arsenal, NJ 07801-5000
2	Commander Production Base Modernization Agency U.S. Army Armament Research, Development, and Engineering Center ATTN: AMSMC-PBM, A. Siklosi AMSMC-PBM-E, L. Laibson Picatinny Arsenal, NJ 07806-5000

No. of Copies	Organization
4	PEO-Armaments Project Manager Tank Main Armament System ATTN: AMCPM-TMA AMCPM-TMA-105 AMCPM-TMA-120 AMCPM-TMA-AS, H. Yuen Picatinny Arsenal, NJ 07806-5000
4	Commander U.S. Army Armament Research, Development, and Engineering Center ATTN: SMCAR-CCH-V, C. Mandala E. Fennell SMCAR-CCH-T, L. Rosendorf SMCAR-CCS Picatinny Arsenal, NJ 07806-5000
18	Commander U.S. Army Armament Research, Development, and Engineering Center ATTN: SMCAR-AEE, J. Lannon SMCAR-AEE-B, A. Beardell D. Downs S. Einstein S. Westley S. Bernstein J. Rutkowski B. Brodman P. O'Reilly R. Cirincione P. Hui J. O'Reilly SMCAR-AEE-WW, M. Mezger J. Pinto D. Wiegand P. Lu C. Hu SMCAR-AES, S. Kaplowitz Picatinny Arsenal, NJ 07806-5000
1	Commander U.S. Army Armament Research, Development and Engineering Center ATTN: SMCAR-HFM, E. Barrieres Picatinny Arsenal, NJ 07806-5000

No. of Copies	Organization
8	Commander U.S. Army Armament Research, Development and Engineering Center ATTN: SMCAR-FSA-F, LTC R. Riddle SMCAR-FSC, G. Ferdinand SMCAR-FS, T. Gora SMCAR-FS-DH, J. Feneck SMCAR-FSS-A, R. Kopmann B. Machek L. Pinder SMCAR-FSN-N, K. Chung Picatinny Arsenal, NJ 07806-5000
3	Director Benet Weapons Laboratories ATTN: SMCAR-CCB-RA, G.P. O'Hara G.A. Pflegl SMCAR-CCB-S, F. Heiser Watervliet, NY 12189-4050
2	Commander U.S. Army Research Office ATTN: Technical Library D. Mann P.O. Box 12211 Research Triangle Park, NC 27709-2211
1	Commander, USACECOM R&D Technical Library ATTN: ASQNC-ELC-IS-L-R, Myer Center Fort Monmouth, NJ 07703-5301
1	Commandant U.S. Army Aviation School ATTN: Aviation Agency Fort Rucker, AL 36360
1	Program Manager U.S. Tank-Automotive Command ATTN: AMCPM-ABMS, T. Dean Warren, MI 48092-2498

No. of Copies	Organization
1	Project Manager U.S. Tank-Automotive Command Fighting Vehicle Systems ATTN: SFAE-ASM-BV Warren, MI 48397-5000
1	Project Manager, Abrams Tank System ATTN: SFAE-ASM-AB Warren, MI 48397-5000
1	Director HQ, TRAC RPD ATTN: ATCD-MA Fort Monroe, VA 23651-5143
1	Commander U.S. Army Belvoir Research and Development Center ATTN: STRBE-WC Fort Belvoir, VA 22060-5006
1	Director U.S. Army TRAC-Ft. Lee ATTN: ATRC-L, Mr. Cameron Fort Lee, VA 23801-6140
1	Commandant U.S. Army Command and General Staff College Fort Leavenworth, KS 66027
1	Commandant U.S. Army Special Warfare School ATTN: Rev and Trng Lit Div Fort Bragg, NC 28307
1	Commander Radford Army Ammunition Plant ATTN: SMCAR-QA/HI LIB Radford, VA 24141-0298
1	Commander U.S. Army Foreign Science and Technology Center ATTN: AMXST-MC-3 220 Seventh Street, NE Charlottesville, VA 22901-5396

No. of Copies	Organization
2	Commandant U.S. Army Field Artillery Center and School ATTN: ATSF-CO-MW, E. Dublisky ATSF-CN, P. Gross Ft. Sill, OK 73503-5600
1	Commandant U.S. Army Armor School ATTN: ATZK-CD-MS, M. Falkovitch Armor Agency Fort Knox, KY 40121-5215
1	U.S. Army Research Development and Standardization Group (UK) PSC 802 Box 15, Dr. Roy E. Richenbach FPO AE09499-1500
2	Commander Naval Sea Systems Command ATTN: SEA 62R SEA 64 Washington, DC 20362-5101
1	Commander Naval Air Systems Command ATTN: AIR-954-Tech Library Washington, DC 20360
4	Commander Naval Research Laboratory ATTN: Technical Library Code 4410, K. Kailasanate J. Boris E. Oran Washington, DC 20375-5000
1	Office of Naval Research ATTN: Code 473, R.S. Miller 800 N. Quincy Street Arlington, VA 22217-9999
1	Office of Naval Technology ATTN: ONT-213, D. Siegel 800 N. Quincy St. Arlington, VA 22217-5000

No. of Copies	Organization
2	Commander Naval Surface Warfare Center ATTN: Code 730 Code R-13, R. Bernecker Silver Spring, MD 20903-5000
7	Commander Naval Surface Warfare Center ATTN: T.C. Smith K. Rice S. Mitchell S. Peters J. Consaga C. Gotzmer Technical Library Indian Head, MD 20640-5000
4	Commander Naval Surface Warfare Center ATTN: Code G30, Guns & Munitions Div Code G32, Guns Systems Div Code G33, T. Doran Code E23 Technical Library Dahlgren, VA 22448-5000
5	Commander Naval Air Warfare Center ATTN: Code 388, C.F. Price T. Boggs Code 3895, T. Parr R. Derr Information Science Division China Lake, CA 93555-6001
1	Commanding Officer Naval Underwater Systems Center ATTN: Code 5B331, Technical Library Newport, RI 02840
1	AFOSR/NA ATTN: J. Tishkoff Bolling AFB, D.C. 20332-6448
1	OLAC PL/TSTL ATTN: D. Shiplett Edwards AFB, CA 93523-5000

No. of Copies	Organization
3	OL-AC PL/RK ATTN: J. Levine L. Quinn T. Edwards 5 Pollux Drive Edwards AFB, CA 93524-7048
1	WL/MNAA ATTN: B. Simpson Eglin AFB, FL 32542-5434
1	WL/MNME Energetic Materials Branch 2306 Perimeter Rd. STE 9 Eglin AFB, FL 32542-5910
1	WL/MNSH ATTN: R. Drabczuk Eglin AFB, FL 32542-5434
2	NASA Langley Research Center ATTN: M.S. 408, W. Scallion D. Witcofski Hampton, VA 23605
1	Central Intelligence Agency Office of Information Resources Room GA-07 HQS Washington, DC 20505
1	Central Intelligence Agency ATTN: J. Backofen NHB, Room 5N01 Washington, DC 20505
1	SDIO/TNI ATTN: L.H. Caveny Pentagon Washington, DC 20301-7100
1	SDIO/DA ATTN: E. Gerry Pentagon Washington, DC 21301-7100
2	HQ DNA ATTN: D. Lewis A. Fahey 6801 Telegraph Rd. Alexandria, VA 22310-3398

No. of Copies	Organization
1	Director Sandia National Laboratories Energetic Materials & Fluid Mechanics Department, 1512 ATTN: M. Baer P.O. Box 5800 Albuquerque, NM 87185
1	Director Sandia National Laboratories Combustion Research Facility ATTN: R. Carling Livermore, CA 94551-0469
1	Director Sandia National Laboratories ATTN: 8741, G. A. Beneditti P.O. Box 969 Livermore, CA 94551-0969
2	Director Lawrence Livermore National Laboratory ATTN: L-355, A. Buckingham M. Finger P.O. Box 808 Livermore, CA 94550-0622
2	Director Los Alamos Scientific Lab ATTN: T3/D. Butler M. Division/B. Craig P.O. Box 1663 Los Alamos, NM 87544
1	Battelle ATTN: TWSTIAC V. Levin 505 King Avenue Columbus, OH 43201-2693
1	Battelle PNL ATTN: M.C.C. Bampton P.O. Box 999 Richland, WA 99352
1	Institute of Gas Technology ATTN: D. Gidaspow 3424 S. State Street Chicago, IL 60616-3896

No. of Copies	Organization
1	Institute for Advanced Technology ATTN: T.M. Kiehne The University of Texas of Austin 4030-2 W. Braker Lane Austin, TX 78759-5329
2	CPIA - JHU ATTN: H. J. Hoffman T. Christian 10630 Little Patuxent Parkway Suite 202 Columbia, MD 21044-3200
1	Brigham Young University Department of Chemical Engineering ATTN: M. Beckstead Provo, UT 84601
1	Jet Propulsion Laboratory California Institute of Technology ATTN: L.D. Strand, MS 125/224 4800 Oak Grove Drive Pasadena, CA 91109
1	California Institute of Technology 204 Karman Lab Main Stop 301-46 ATTN: F.E.C. Culick 1201 E. California Street Pasadena, CA 91109
3	Georgia Institute of Technology School of Aerospace Engineering ATTN: B.T. Zim E. Price W.C. Strahle Atlanta, GA 30332
2	University of Illinois Department of Mechanical/Industry Engineering ATTN: H. Krier R. Beddini 144 MEB; 1206 N. Green St. Urbana, IL 61801-2978
1	University of Massachusetts Department of Mechanical Engineering ATTN: K. Jakus Amherst, MA 01002-0014
1	University of Minnesota Department of Mechanical Engineering ATTN: E. Fletcher Minneapolis, MN 55414-3368
3	Pennsylvania State University Department of Mechanical Engineering ATTN: V. Yang K. Kuo C. Merkle University Park, PA 16802-7501
1	Rensselaer Polytechnic Institute Department of Mathematics Troy, NY 12181
1	Stevens Institute of Technology Davidson Laboratory ATTN: R. McAlevy III Castle Point Station Hoboken, NJ 07030-5907
1	Rutgers University Department of Mechanical and Aerospace Engineering ATTN: S. Temkin University Heights Campus New Brunswick, NJ 08903
1	University of Utah Department of Chemical Engineering ATTN: A. Baer Salt Lake City, UT 84112-1194
1	Washington State University Department of Mechanical Engineering ATTN: C.T. Crowe Pullman, WA 99163-5201

No. of Copies	Organization
1	AFELM, The Rand Corporation ATTN: Library D 1700 Main Street Santa Monica, CA 90401-3297
1	Arrow Technology Associates, Inc. ATTN: W. Hathaway P.O. Box 4218 South Burlington, VT 05401-0042
3	AAI Corporation ATTN: J. Hebert J. Frankle D. Cleveland P.O. Box 126 Hunt Valley, MD 21030-0126
2	Alliant Techsystems, Inc. ATTN: R.E. Tompkins J. Kennedy 7225 Northland Dr. Brooklyn Park, MN 55428
1	AVCO Everett Research Laboratory ATTN: D. Stickler 2385 Revere Beach Parkway Everett, MA 02149-5936
1	General Applied Sciences Lab ATTN: J. Erdos 77 Raynor Ave. Ronkonkama, NY 11779-6649
1	Martin Marietta Tactical System Department ATTN: J. Mandzy 100 Plastics Ave. Pittsfield, MA 01201-3698
1	IITRI ATTN: M.J. Klein 10 W. 35th Street Chicago, IL 60616-3799
4	Hercules, Inc. Radford Army Ammunition Plant ATTN: L. Gizzi D.A. Worrell W.J. Worrell C. Chandler Radford, VA 24141-0299
2	Hercules, Inc. Allegheny Ballistics Laboratory ATTN: William B. Walkup Thomas F. Farabaugh P.O. Box 210 Rocket Center, WV 26726
1	Hercules, Inc. Aerospace ATTN: R. Cartwright 100 Howard Blvd. Kenville, NJ 07847
1	Hercules, Inc. Hercules Plaza ATTN: B.M. Riggleman Wilmington, DE 19894
1	MBR Research Inc. ATTN: Dr. Moshe Ben-Reuven 601 Ewing St., Suite C-22 Princeton, NJ 08540
1	Olin Corporation Badger Army Ammunition Plant ATTN: F.E. Wolf Baraboo, WI 53913
3	Olin Ordnance ATTN: E.J. Kirschke A.F. Gonzalez D.W. Worthington P.O. Box 222 St. Marks, FL 32355-0222
1	Olin Ordnance ATTN: H.A. McElroy 10101 9th Street, North St. Petersburg, FL 33716
1	Paul Gough Associates, Inc. ATTN: P.S. Gough 1048 South St. Portsmouth, NH 03801-5423
1	Physics International Library ATTN: H. Wayne Wampler P.O. Box 5010 San Leandro, CA 94577-0599

No. of Copies	Organization
2	Princeton Combustion Research Laboratories, Inc. ATTN: N. Mer N.A. Messina Princeton Corporate Plaza 11 Deerpark Dr., Bldg IV, Suite 119 Monmouth Junction, NJ 08852
3	Rockwell International Rocketdyne Division ATTN: BA05, J. Flanagan J. Gray WC79, R. Edelman 6633 Canoga Avenue Canoga Park, CA 91303-2703
2	Rockwell International Science Center ATTN: Dr. S. Chakravarthy Dr. S. Palaniswamy 1049 Camino Dos Rios P.O. Box 1085 Thousand Oaks, CA 91360
1	Science Applications International Corp. ATTN: M. Palmer 2109 Air Park Rd. Albuquerque, NM 87106
1	Southwest Research Institute ATTN: J.P. Riegel 6220 Culebra Road P.O. Drawer 28510 San Antonio, TX 78228-0510
1	Sverdrup Technology, Inc. ATTN: Dr. John Deur 2001 Aerospace Parkway Brook Park, OH 44142
3	Thiokol Corporation Elkton Division ATTN: R. Willer R. Biddle Tech Library P.O. Box 241 Elkton, MD 21921-0241
1	Veritay Technolcgy, Inc. ATTN: E. Fisher 4845 Millersport Hwy. East Amherst, NY 14501-0305

No. of Copies	Organization
1	Universal Propulsion Company ATTN: H.J. McSpadden 25401 North Central Ave. Phoenix, AZ 85027-7837
1	SRI International Propulsion Sciences Division ATTN: Tech Library 333 Ravenwood Avenue Menlo Park, CA 94025-3493
	Aberdeen Proving Ground
1	Cdr, USACSTA ATTN: STECS-PO/R. Hendricksen

No. of Copies	Organization
1	Ernst-Mach-Institut ATTN: Dr. R. Heiser Haupstrasse 18 Weil am Rheim Germany
1	Defence Research Agency, Military Division ATTN: C. Woodley RARDE Fort Halstead Sevenoaks, Kent, TN14 7BP England
1	School of Mechanical, Materials, and Civil Engineering ATTN: Dr. Bryan Lawton Royal Military College of Science Shrivenham, Swindon, Wiltshire, SN6 8LA England
2	Institut Saint Louis ATTN: Dr. Marc Giraud Dr. Gunther Sheets Postfach 1260 7858 Weail am Rhein 1 Germany
1	Explosive Ordnance Division ATTN: A. Wildegger-Gaissmaier Defence Science and Technology Organisation P.O. Box 1750 Salisbury, South Australia 5108
1	Armaments Division ATTN: Dr. J. Lavigne Defence Research Establishment Valcartier 2459, Pie XI Blvd., North P.O. Box 8800 Courcelette, Quebec G0A 1R0 Canada

USER EVALUATION SHEET/CHANGE OF ADDRESS

This Laboratory undertakes a continuing effort to improve the quality of the reports it publishes. Your comments/answers to the items/questions below will aid us in our efforts.

1. ARL Report Number ARL-CR-126 Date of Report April 1994

2. Date Report Received _____

3. Does this report satisfy a need? (Comment on purpose, related project, or other area of interest for which the report will be used.) _____

4. Specifically, how is the report being used? (Information source, design data, procedure, source of ideas, etc.) _____

5. Has the information in this report led to any quantitative savings as far as man-hours or dollars saved, operating costs avoided, or efficiencies achieved, etc? If so, please elaborate. _____

6. General Comments. What do you think should be changed to improve future reports? (Indicate changes to organization, technical content, format, etc.) _____

CURRENT ADDRESS

_____
Organization

_____
Name

_____
Street or P.O. Bcx No.

_____
City, State, Zip Code

7. If indicating a Change of Address or Address Correction, please provide the Current or Correct address above and the Old or Incorrect address below.

OLD ADDRESS

_____
Organization

_____
Name

_____
Street or P.O. Box No.

_____
City, State, Zip Code

(Remove this sheet, fold as indicated, tape closed, and mail.)
(DO NOT STAPLE)

DEPARTMENT OF THE ARMY

OFFICIAL BUSINESS

BUSINESS REPLY MAIL
FIRST CLASS PERMIT No 0001, APG, MD

Postage will be paid by addressee.

Director
U.S. Army Research Laboratory
ATTN: AMSRL-OP-CI-B (Tech Lib)
Aberdeen Proving Ground, MD 21005-5066

NO POSTAGE
NECESSARY
IF MAILED
IN THE
UNITED STATES